Contents lists available at ScienceDirect

Ore Geology Reviews

journal homepage: www.elsevier.com

Review

The structural setting of mineralisation at Kolomela Mine, Northern Cape, South Africa, based on fully-constrained, implicit 3D modelling

I.J. Basson[a, d], S.A.J. Thomas[a, *], B. Stoch[a], C.J. Anthonissen[a], M-J. McCall[a], J. Britz[c], S. Macgregor[c], S. Viljoen[b], D. Nel[c], M. Vietze[b], C. Stander[b], J. Horn[b], J. Bezuidenhout[b], T. Sekoere[b], C. Gous[b], H. Boucher[c]

[a] Tect Geological Consulting, Unit 3, Metrohm House, Gardner-Williams Avenue, Paardevlei, Somerset West 7130, South Africa
[b] Kolomela Mine, 21 Main Street, Postmasburg, 8420, South Africa
[c] Kumba Iron Ore, Corporate Office, Centurion Gate, 124 Akkerboom Road, Centurion, 0157, South Africa
[d] Department of Earth Sciences, Stellenbosch University, Private Bag X1, Matieland, Stellenbosch, 7602, South Africa

ARTICLE INFO

ABSTRACT

Kolomela Mine, formerly known as the Sishen South Project, is located approximately 9 km from Postmasburg, in the Northern Cape Province of South Africa. Iron ore is primarily concentrated near the top of the Asbesheuwels or Asbestos Hills Subgroup, within the Kuruman Formation. High-grade, hematite-rich, iron-ore deposits in South Africa have been addressed in the literature, although much of this work focusses on their geochemical or isotopic signatures and the role of paleosinkholes in ore preservation. Recent work on high-grade, BIF-hosted Fe deposits, in South Africa and elsewhere, emphasizes the role of deformation in iron mineralisation and upgrading of BIF over a sequence of events, either punctuated by supergene enrichment or terminating with a supergene overprint. The proximity of the Kheis orogenic front, the protracted tectonic history of the area, a recently-resolved local structural framework and an emerging set of literature on superimposed hypogene, metasomatic, hydrothermal, hypothermal and deformation-induced processes, justify a re-examination of the Kolomela deposits. Closely-spaced drillhole data, pit mapping over a period of four years and re-interpretation of the tectonic setting from high-resolution geophysical data, have been incorporated into fully-constrained 3D models of the five principle Kolomela deposits, which are presented here and analysed in terms of their geometry, tectonic setting, relationship to major structures, the geometry of the underlying dolomite contact and the possible role of gabbroic intrusions. A strong spatial correlation between thicker ore and thicker, underlying gabbroic bodies, in the forms of sills, is evident. We propose that protracted, multi-phase tectonic evolution, complete with several compressional-extensional events at this margin of the Kaapvaal Craton provided an ideal setting for "preparation" of BIF by early low-grade metamorphism, deformation and porosity creation, followed by fluid movement along interconnected contacts, unconformities, gabbro contacts and major structures.

1. Introduction

Kolomela Mine, formerly known as the Sishen South Project, is located approximately 9 km from Postmasburg, in the Northern Cape Province of South Africa. The mine produces direct shipping iron ore and as of November 2011, it contained 101.3 Mt of proven reserves grading at 64.4% Fe and 98.7 Mt of probable reserves grading at 64.5% Fe. The mine consists of several separate deposits: Kapstevel North (KSN), Kapstevel South (KSS), Leeuwfontein (LF), Klipbankfontein (KF) and Ploegfontein (PF), of which KSN, LF and KF are presently mined. The deposits consist of competent, massive ore, laminated ore and conglomeratic ore and the bulk of mineralisation comprises granular and microplaty hematite with specularite veining. Commercial production commenced in 2011 and the operation has an estimated mine life of at least 29 years.

Kolomela Mine is situated at the southern termination of a range of low hills, with 60 km of strike extent, along the western limit of the Maremane Anticline or Maremane Dome. This dome is rimmed by lithologies of the Griqualand West and Olifantshoek Supergroups (Fig. 1) and the deposits are generally cited as being hosted in a Lake Superior-type banded iron formation (Gross, 1993; Beukes and Gutzmer,

* Corresponding author.
Email address: sukey.thomas@gmail.com (S.A.J. Thomas)

https://doi.org/10.1016/j.oregeorev.2018.02.032
Received 26 July 2017; Received in revised form 24 January 2018; Accepted 23 February 2018
Available online xxx
0169-1368/

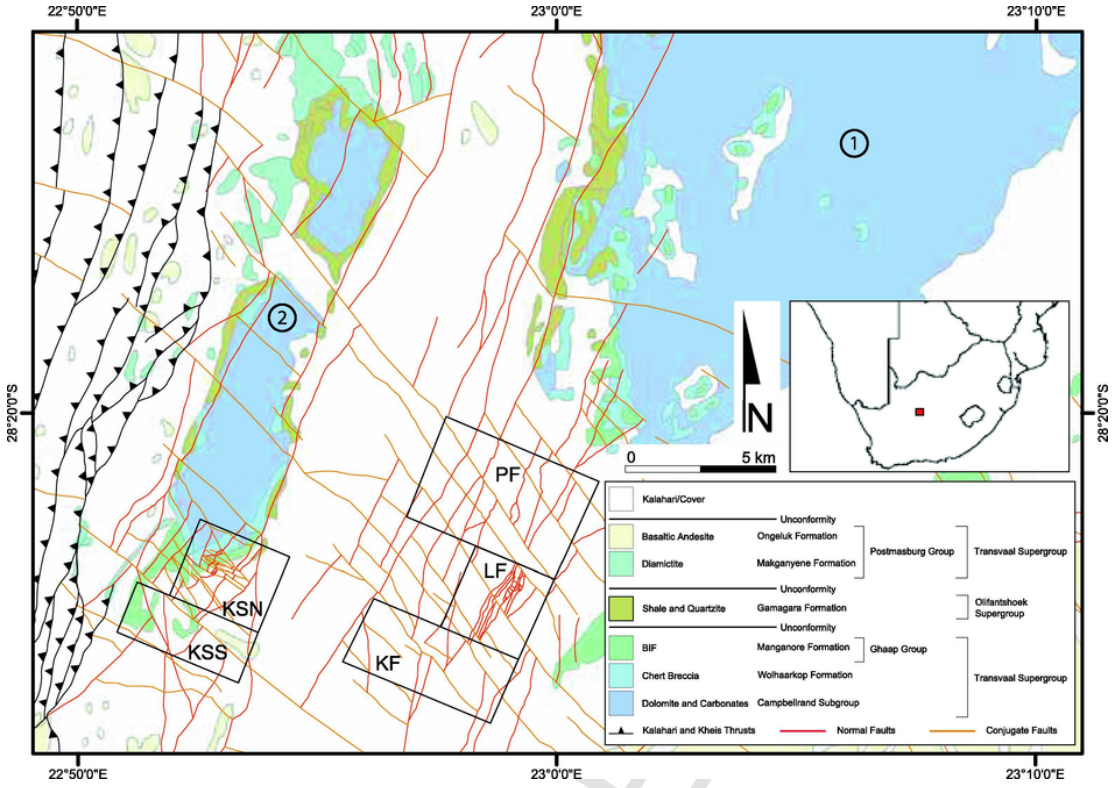

Fig. 1. Regional geological map of the Kolomela area, with regional structural features and 3D model limits. KSN –Kapstevel North; KSS – Kapstevel South; LF – Leeuwfontein; KF – Klipbankfontein; PF- Ploegfontein; 1 – Maremane Dome; 2 – Wolhaarkop Dome.

2008), which formed in a passive-margin setting. Ore is primarily concentrated near the top of the Asbesheuwels or Asbestos Hills Subgroup, within the Kuruman Formation. Approximately 80% of Kolomela is covered by sand, dolocrete and calcrete of the Kalahari Group. Early geophysical surveys and exploration drilling delineated several covered anomalies in the central and eastern portions of the prospecting area, with iron ore cropping out on the western portion of Welgevonden 486 and Kapstevel 451 (Alchin et al., 2008). Iron mineralisation in this stratigraphic sequence in South Africa has been variably attributed to several processes or models, primarily supergene (Wagner, 1921; Boardman, 1948; Van Deventer, 2009) or supergene-metamorphic, "ancient" supergene (Beukes, 1983; Beukes et al., 2002), magmatically-driven (e.g. De Villiers, 1944), metasomatic-hydrothermal with a supergene overprint (Du Preez, 1944; Strauss, 1964; Van Deventer et al., 1986; Beukes et al., 2002), low-temperature hydrothermal (Papadopoulos, 2016) or hypothermal processes during fold amplification in fold-and-thrust belts, for example on the northern margin of the basin around Thabazimbi (Basson and Koegelenberg, 2016). Syngenetic models have not been extensively proposed for the deposits rimming the Maremane Dome, although the basin geometry and its faults show many similarities to other mineralized terrains. Such models cite the influence of synsedimentary, *syn*-dewatering or loading structures, such as normal faults or extensional boudinage (Findlay, 1994). High-grade, hematite-rich, iron-ore deposits such as Kolomela have been addressed in the literature, although much of this work focusses on their geochemistry or isotopic signatures (e.g. Barley et al., 1999; Taylor et al., 2001; Gutzmer et al., 2006, 2008; Rosière et al., 2008; Ramanaidou and Morris, 2010).

Contributions by Alchin and Botha (2005), Friese and Alchin (2007) and Alchin et al. (2008) provided preliminary observations on the structural setting of these deposits. These publications were some of the first to depict a relationship between structures and ore, illustrated using schematic or interpreted cross-sections, the latter based on preliminary 3D models. Subsequent work on high-grade, BIF-hosted Fe deposits increasingly emphasized the role of deformation in iron mineralisation and upgrading of BIF over a sequence of events (e.g. Taylor et al., 2001; Angerer and Hagemann, 2010; Lascelles, 2012), either punctuated by supergene enrichment or terminating with a supergene overprint. Such studies have already raised questions regarding the accepted ages and events in the upper parts of the sequence. For instance, Fairey et al. (2012) studied the Mooidraai carbonates, which overly the Hotazel Formation of the Postmasburg Group of the Transvaal Supergroup. The resolved localized metasomatic overprint affected the U–Pb isotopic signature, involving U gain at the end of the Neoproterozoic. In a geochemical study on the Hotazel Formation (close to Sishen mine), Tsikos et al. (2003) identified the geochemical effects of an isotopically light fluid, which they proposed was either meteoric water or a low-temperature hydrothermal fluid, in the oxidation, leaching and enrichment of iron. On this basis, they proposed that extensive fluid flow in the Kalahari manganese field was related to the Hotazel/Olifantshoek unconformity at the top of the Transvaal/Griqualand West Supergroup and therefore above the stratigraphic location of Sishen Mine. In a similar vein, work by Lacselles (2002) suggests that hematite deposits in analogue terrains (e.g. the Hamersley and Yilgarn Provinces) cannot be attributed to – let alone solely attributed to - leaching of quartz from laminated cherty BIF during supergene processes.

The proximity of Kolomela to the Kheis orogenic front as well as the protracted tectonic history of the area, the recently resolved local structural framework and an emerging set of literature on superimposed hypogene, metasomatic, hydrothermal, hypothermal and deformation-induced processes justify a re-examination of the Kolomela deposits. Recently, fully-constrained 3D models of the five principle Kolomela deposits were constructed as part of an ongoing project to adopt implicit modelling. These models incorporate closely-spaced drillhole data, pit mapping over a period of four years, a re-interpreta-

tion of the tectonic setting of this part of the Maremane Dome and high-resolution geophysical data. This contribution aims to provide a systematic analysis of each deposit in terms of its geometry, tectonic setting and its relationship to major structures, the underlying dolomite contact and gabbroic intrusions. A subsidiary aim is to compare Kolomela to other, well-documented deposits globally (e.g. Hagemann et al., 2016) and to encourage further research on mineralisation processes that may have preceded uplift, exhumation, weathering and possibly final upgrading of Fe mineralisation by supergene alteration, as detailed in Lascelles (2002, 2007), Bekker et al. (2010), Hagemann et al. (2016) and Rasmussen et al. (2016).

2. Geology of the Maremane Dome

2.1. Regional structural evolution

This portion of the southwestern to western Kaapvaal Craton and its overlying sequences have undergone polyphase deformation, according to van Schalkwyk and Beukes (1986), Stowe (1986), Hilliard (1999), Carney and Mienie (2003), Friese and Alchin (2007), Altermann and Hälbich (1991) and Beukes and Smit (1987). Hälbich et al. (1993) and Hilliard (1999) refer to extensive deformation in the lower portions of the Transvaal Supergroup and its ore-bearing zones. The deformational history and the lithologies and structures related to each event are summarized in Table 1.

The formation of the Ventersdorp Rift Basin around 2.78–2.64 Ga initiated with the deposition of the Campbellrand dolomite, Wolhaarkop chert and BIF of the Ghaap Group, followed by a series of orogenic events, separated by hiatuses or extensional events. A new baddeleyite U-Pb age of 2442 ± 5 Ma was obtained for the intracratonic Westerberg sill, which intruded banded iron formation of the Kuruman Formation of the Transvaal Supergroup to the south of Kolomela, displaying folding that trends tangentially to the Maremane Dome (Kampmann, 2012). The ~2.35–2.25 Ga east-verging Kalahari Orogeny formed N—S trending F_1 folds, generated the Uitkomst cataclasite (Altermann and Hälbich, 1991) and inverted rift-related faults. Uplift and erosion of lithologies at this time, including those of the Ghaap Group, led to the formation of the Postmasburg Unconformity, commonly cited as being instrumental in supergene Fe-enrichment models. Between ~2.24 and 1.83 Ga, reactivation of rift-related faults caused deposition of the volcanosedimentary to volcaniclastic Upper Postmasburg Group. Ongeluk lavas mark the peak of mafic lava extrusion at *c.* ~2.22 Ga. Deposition of clastic sediments in the form of conglomerate, "grit", quartzite and shale of the lower Olifantshoek Supergroup took place at ~2.05–1.93 Ga, thereby forming the Gamagara/Mapedi Formation within shallow-water rifts (Beukes, 1983). The emplacement of the Hartley Large Igneous Province, to form the Hartley Formation, took place at 1923 ± 6 Ma to 1915.2 ± 1.1 Ma (Semami et al., 2016; Cornell et al., 2016). The Eburnean or E2 extensional event (Dalstra and Rosière, 2008) resulted in reactivated normal faults displacing or offsetting the lower Olifantshoek Supergroup.

South-verging folds and thrusts, according to Altermann and Hälbich (1991), occurred between 2.07 and 1.88 Ga. From 1.83 to 1.73 Ga, the Kheis or Kheis-Koranna Orogeny or tectonometamorphic event, like the Kalahari Orogeny, showed eastward tectonic vergence, thrusting, folding (Stowe, 1986; Beukes and Smit, 1987; Altermann and Hälbich, 1991; Hälbich et al., 1993; Hilliard, 1999) and inversion or further inversion of older, long-lived normal faults. Rift structures of the Postmasburg Group and Olifantshoek Supergroup depositional settings were reactivated and inverted, while F_2 folding and thin-skinned thrusting occurred along major unconformities, lithological contacts and the Blackridge Thrust at the base of the lower Ongeluk lavas and Makganyene diamictite. The Groblershoek Schist Formation of the Olifantshoek Supergroup yields an ^{39}Ar-^{40}Ar metamorphic age of ~1780 Ma (Schlegel; 1988) and constrains the age of the Kheis Orogeny, which resulted in numerous deformational features within the Griqualaland West Supergroup (Hilliard, 1999; Table 1). Possibly Bushveld-age gabbroic rocks intruded the Ghaap and Postmasburg Groups, a process partly accommodated by the reactivation of Ventersdorp faults (Friese and Alchin, 2007).

The third orogenic event, to the south of the Kolomela area, comprises the ~1.35–1.0 Ga NNW-directed Lomanian (Namaqua-Natal) Orogeny, which caused deformation along the southern margin of the Kaapvaal Craton (Altermann, 1997; ^{39}Ar-^{40}Ar metamorphic age; Altermann and Hälbich, 1990, 1991). This formed a large-scale, dextral shear system, which shows numerous, parallel, smaller-scale, right-lateral shears to the north of it. The effects of this event are manifold: reactivation, segmentation and buckling of N—S trending normal and inverted normal faults; reactivation of the 2.35–2.24 Ga NE- and SE-trending, conjugate, strike-slip faults, usually with uplift to the SE and SW, respectively, and the development of ENE-trending F_3 folds (this study). This event was probably responsible for an overall northward dip of approximately 3° across the Maremane Dome and the emplacement of magnetite along major NW-SE trending faults (e.g.. the Griquatown Fault Zone; Erikson et al., 2006). The Lomanian Orogeny also caused broad F_2/F_3 fold interference patterns (Hilliard, 1999; Mortimer, 1995), particularly in units above the Blackridge Thrust, best observed at Sishen Mine (Basson et al., 2017), as well as refolding, segmentation and buckling of thrusts, normal faults and inverted normal faults. The "asymmetry" of the Maremane Dome, mimicked on a smaller scale by the Wolhaarkop Dome to the west of its southern termination, may have partly resulted from dextral shearing in the Namaquan part of the Namaqua-Natal Orogeny. Subsequent tectonism, including the breakup of Gondwana and Pan-African reworking, appear to have had only a minor effect on the region.

2.2. Stratigraphy

The Griqualand West Basin of the Transvaal Supergroup is well-preserved in the Northern Cape of South Africa (Fig. 1). The base of the Ghaap Group (Transvaal Supergroup) comprises the *ca.* 2.6–2.43 Ga Campbellrand Subgroup (Eriksson et al., 1993; Moore et al., 2000), conformably overlying the Schmidtsdrif Subgroup. Important age constraints are provided by two tuffaceous volcanic horizons; one 50 m below the basal contact of the Asbestos Hills Subgroup (2521 ± 3 Ma; Sumner and Bowring, 1996; U-Pb single zircon TIMS age) and another 150 m below this contact (2552 ± 12 Ma; Barton et al., 1994; U-Pb single zircon SHRIMP age).

The Wolhaarkop Breccia or Wolhaarkop Formation, which unconformably overlies dolomite, is a siliceous chert breccia, locally enriched in manganese and/or hematite and comprising angular to subrounded chert fragments in a grey-brown chert matrix. Van Wyk (1980) and Van Schalkwyk and Beukes (1986) suggest an exposed, relict, karstic topography accompanied by solution-collapse in a periodically-exposed shallow-water setting (Moore et al., 2011). The Wolhaarkop Formation grades upwards into undisturbed or partly brecciated and folded ironstones of the Manganore Formation (Van Schalkwyk and Beukes, 1986), which is the local term for the Kuruman Iron Formation, occasionally interlayered with shale of the *ca.* 2.52–2.43 Ga Asbestos Hills Subgroup (Beukes, 1983; Van Schalkwyk and Beukes, 1986). Volcanic tuff in the Griquatown Formation, which is mostly absent from the Kolomela area, has been dated at 2432 ± 31 Ma (Trendall et al., 1990; U-Pb single zircon SHRIMP). The upper portion of the Manganore/Kuruman Iron Formation shows Fe enrichment to ore grade.

The Gamagara/Mapedi Formation (Beukes and Smit, 1987) has an age of *ca.* 2.05–1.83 Ga and overlies banded iron formation at an un-

Table 1
Summary of the tectonostratigraphic history of the Kolomela area, with lithologies and structures related to each event.

Period	Event	Lithologies	Structural Features	Sources/Comparative Studies
~2.78–2.64 Ga	Ventersdorp Rift Basin initiation and subsidence, volcanism;	Extrusion and deposition of Volcanosedimentary Vryburg Formation and Ventersdorp Lavas	NE-SW normal faults formed graben boundaries	
~2.60–2.465 Ga	Development of carbonate platform followed by widespread marine transgression;	Schmidtsdrif and Campbellrand Subgroup dolomites		
~2.46–2.35 Ga	Deposition of Mn-chert, followed by deposition of the Asbestos Hills Subgroup (Manganore iron formation); Incipient break-up and rifting along N—S trending, W-dipping normal faults during a "second extensional stage";	Chert, BIF, laminated and massive ore		Friese and Alchin (2007)
~2.35–2.25 Ga:	E-verging Kalahari orogeny leads to N—S trending F_1 folds (e.g. Maremane Dome). Uplift and erosion of underlying units to form Postmasburg Unconformity, which is cited as pivotal for supergene Fe enrichment; Reactivation and inversion of pre-existing, rift-related normal faults; formation of conjugate NE- and SE-trending, strike-slip faults	(uplift and erosion) Makganyene Formation, (continental glacial deposits attributed to "snowball earth") Minimum age of 2.22 Ga	N—S trending F_1 folds, inverted normal faults, NE- and SE-trending strike-slip faults	>2.24 Ga or pre-Makganyene development of the Uitkomst cataclasite, attributed to bedding-parallel thrusting (Altermann and Hälbich, 1991)
~2.24–1.83 Ga	Reactivation of N—S trending passive margin rift and Ventersdorp Rift, leading to volcanism and deposition of volcanic sediments in fault-bounded grabens; Deposition of Olifantshoek Supergroup (~2.05–1.93 Ga), including Gamagara/Mapedi Formation, in shallow-water rift environment; Emplacement of the Hartley LIP at 1923 ± 6 Ma to 1915 ± 1.1 Ma; Reactivated normal faults offset lower Olifantshoek Supergroup, development of south-verging folds and thrusts;	Ongeluk Lavas signify peak mafic lava extrusion at ~2.22 Ga. Hartley Formation/ LIP Gamagara Formation: Conglomerate, grit, quartzite and shale	NNE- to NE-trending faults exploited by volcanism	Cornell et al., 1996; Friese and Alchin, 2007; Beukes, 1983; Altermann and Hälbich, 1991 Semami et al. (2016), Cornell et al. (2016) Formation of south-verging folds and thrusts, which, according to Altermann and Hälbich (1991), are the oldest post-Matsap event at 2.07–1.88 Ga;
1.83–1.73 Ga	Kheis or Kheis-Koranna Orogeny: eastward tectonic vergence accompanied by thrusting and folding; Reactivation of rift structures relating to Postmasburg Group and Olifantshoek Supergroup depositional settings; F2 folding and thin-skinned thrusting along major uncomformities and lithological contacts (including Blackridge Thrust); Co-axial tightening of F1 folds. Kheis Orogeny is more precisely dated at ~1780 Ma by ^{39}Ar-^{40}Ar metamorphic age derived from Groblershoek Schist Formation of Olifantshoek Supergroup; Supergene Fe enrichment and hydrothermal Fe mineralisation;		F_1 folds tightened by F_2 folding; N—S trending, west-dipping thin-skinned thrust planes along major uncomformities e.g. Blackridge Thrust at base of Ongeluk Lava /Makganyene Diamictite Deformation in Griqualand West Supergroup: shearing along contact with Olifantshoek Supergroup; shearing and rotation of bedding in vicinity of major thrusts and bedding sub-parallel simple shear in Asbestos Hills and Koegas Subgroups.	Stowe, 1986; Beukes and Smit, 1987; Altermann and Hälbich, 1991; Hälbich et al., 1993; Hilliard, 1999 Tinker et al., 2002 Schlegel, 1988 (^{39}Ar-^{40}Ar metamorphic age)
~1.35–1.0 Ga	NNW-directed Lomanian (Namaqua-Natal) Orogeny; Deformation along southern margin of Kaapvaal Craton: Reactivation, segmentation and buckling of N—S trending normal and inverted normal faults; Reactivation of NE- and SE-trending conjugate strike-slip faults (formed during Kalahari orogeny) and development of ENE-trending F3 folds; Possible contribution to broad F2/F3 fold interference patterns; Reactivation of early faults by NW- to NNW-striking, oblique, dextral strike slip faults, such as the Dagbreek Fault;	Koras Group sediments and volcanosediments deposited locally in pull-apart basins bordered by faults	ENE-trending F3 folds; F2/F3 fold interference patterns; NW- to NNW-striking, oblique dextral strike slip faults (e.g. Dagbreek Fault)	Altermann, 1997 (^{39}Ar-^{40}Ar metamorphic age). Stowe (1986) Hilliard (1999); Mortimer (1995) Hartnady et al. (1985); Thomas et al. (1994)

conformable contact. It consists of a thick sequence of younger clastic sediments, including shale, quartzite and conglomerate. Hematitic conglomerate, which marks the base of the Olifantshoek Supergroup, typically constitutes lower-grade ore at the eroded upper contact of the Manganore/Kuruman Iron Formation. The unconformity represents approximately 380 myr of erosion and uplift, between 2.43 Ga and 2.05 Ga, at the Manganore Iron Formation-Gamagara/Mapedi Formation contact. Due to its deposition on a densely-faulted footwall, the Gamagara/Mapedi Formation varies greatly in thickness or is completely absent.

West of the Maremane Dome, diamictite of the Makganyene Formation (de Villiers and Visser, 1977) and basaltic andesite/andesite of the Ongeluk Formation (both part of the Postmasburg Group) were thrust eastwards over Gamagara Formation sediments, along what has been interpreted as a thrusted unconformity or tectonic unconformity, termed the Blackridge Thrust (Beukes and Smit, 1987) or Makganyene Unconformity. This feature is one of several forward-propagating splays that have created thin klippe or outliers within the foreland of the thrust front. These units are primarily preserved in synclines flanking the Wolhaarkop Dome (Schütte, 1992), but have been removed by erosion over up-faulted, anticlinal or domal areas, thereby exposing dolomite. Tholeiitic basaltic andesite of the Ongeluk Formation, extruded underwater in a marginal basin of the Kaapvaal Craton (Schütte, 1992), yields ages of 2240 ± 57 Ma (Walraven et al., 1982), 2239 ± 90 Ma (Armstrong, 1987) and 2222 ± 13 Ma (Cornell et al., 1996; U-Pb whole rock analysis). The age of the Ongeluk lavas effectively assigns a maximum age to the Mapedi Formation, which postdates the Great Oxidation event (GOE; see Bekker et al., 2004) by a minimum of 100 myr. Shale, of the Sishen Member in the Gamagara Formation, is generally overlain by purplish-white Marthaspoort quartzite followed by further green to red shales of the uppermost Paling Member. The region hosting the Mapedi Formation has experienced only low-grade metamorphism, with maximum temperatures of 110–170 °C and pressures less than 2 kbar (Miyano and Beukes, 1984).

Makganyene diamictite is massive to poorly-bedded and contains lenses of pebbly sandstone, siltstone, shale and mudstone, interpreted as piedmont glacial and glaciofluvial assemblages by Beukes (1983) and Visser (1971). Dwyka glaciation removed a significant interval of the stratigraphy and redeposited this as tillite (Visser, 1971), notably preserved in the Kapstevel North/South and Leeuwfontein model volumes, during the Cretaceous. Tertiary regional erosion produced calcrete, dolocrete, clay and pebble layers of the Kalahari Group, deposited unconformably over older lithologies; however, this cover is extremely thin to completely absent in the Kolomela area.

Several diabase dykes and sills occur in the region. Carney and Mienie (2003) noted significant gabbroic sills that separate iron ore from the banded iron formation. Kapstevel South shows at least two gabbroic sills that transgress the orebody, while Leeuwfontein contains an extensive and laterally-persistent sill that consistently underlies the main orebody across its full extent. Friese and Alchin (2007) suggested that gabbro intruded into the Griqualand West Supergroup during the late Proterozoic.

2.3. Geometry of regional dolomite surface

Based on the distribution of known deposits around the Maremane Dome and other parts of the Griqualand West Supergroup, the dolomite's upper contact, at which the Wolhaarkop Breccia is situated, forms an important marker. This is not only due to the formation of sinkholes and palaeosinkholes at this level, but also because its geometry and depth reflect the cumulative effects of the various deformation events in the Kolomela area. A separate hydrological study resulted in a regional 3D model of the top dolomite contact using; a) fixed constraints such as intersections extracted from drillhole data; b) the base of the conductive Manganore package from Spectrem CDI sections; c) mapped 100 k geology outcropping contacts and d) 3D mine-scale geological models (Wooldridge and Hobson, 2015).

The regional dolomite surface shows two broad, NNE-SSW-trending, doubly-plunging anticlines. The larger of these is the Maremane Dome, the southern termination of which overlaps with the Kolomela area and the Ploegfontein, Leeuwfontein and Klipbankfontein deposits (see Fig. 2). Kapstevel North and Kapstevel South are situated at the southern

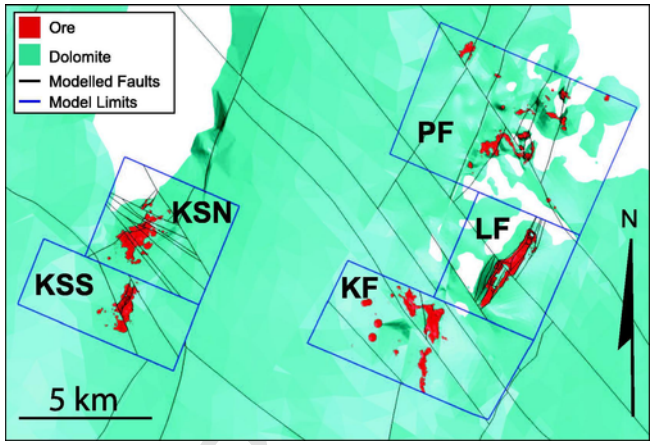

Fig. 2. Plan view of modelled ore volumes, in the context of the underlying modelled dolomite surface, with fault network and model limits displayed as traces.

termination of the smaller Wolhaarkop Dome to the west. Extensive NE-trending normal faults transect the area and reactivated/inverted normal faults parallel the limbs of anticlines and domes. The eastern extent or front of the Kheis Orogeny occurs approximately 2 km to the west of the Kapstevel deposits (KSS and KSN on Fig. 1).

2.4. BIF and ore types

A BIF-hosted iron ore system is located in (or largely derived from) BIF, which is defined, according to Beukes and Gutzmer (2008), as "a variety of iron formation that contains distinct chert layers, known as bands; iron formation is a finely laminated to thinly bedded, chert-bearing chemical sedimentary rock containing at least 15 wt% iron of sedimentary origin". BIF comprises alternating millimetre- to centimetre-scale, iron-rich (typically iron oxide) and iron-poor (typically chert) microbands and mesobands. The presence or absence of chert bands earns the moniker of cherty BIF or chert-free BIF, respectively.

Two main ore types are commonly described for Maremane Dome deposits; a) hard, microcrystalline hematite, formed by supergene enrichment of Asbestos Hills Subgroup BIF below the Gamagara unconformity; b) conglomeratic or detrital ores formed by laminated ore erosion and accumulation in depressions in the Gamagara Formation, interbanded with high-Al, diaspore-rich shale and pisolitic-lateritic horizons (Van Schalkwyk and Beukes, 1986; Gutzmer and Beukes, 1998). Ore types at Kolomela Mine were initially thought to be similar to those at Sishen Mine, although there are distinct differences in their chemistry, physical properties, metallurgical properties (Carnie and Mienie, 2003), proportions and geometries (this study). Alchin et al. (2008) assigned ore at Kolomela to four sub-types a) laminated hematite ± specular hematite; b) clastic-textured; c) collapse-breccia and d) conglomeratic. However, up to six ore types are routinely recorded in drillhole logging at Kolomela (Fig. 3), with intervals being classified according to their texture and inferred genesis (laminated, massive, clastic, conglomeritic, brecciated and detrital). These ore types and their grades vary greatly over short distances and between deposits, which complicates grade control and ore tracking (see Steynfaard et al., 2003). For modelling purposes, these textural types were grouped into three dominant ore types: laminated, conglomeritic and clastic (incorporating massive and detrital). Brecciated ore is uncommon in most deposits and is generally grouped with clastic ore, with the exception of Ploegfontein, which - due to its numerous paleosinkholes - contains sufficient intersections and thereby volumes of brecciated or collapsed ore to warrant their modelling.

Laminated ore comprises alternating microbands of higher- and lower-luster hematite interspersed with hematite and specularite bands

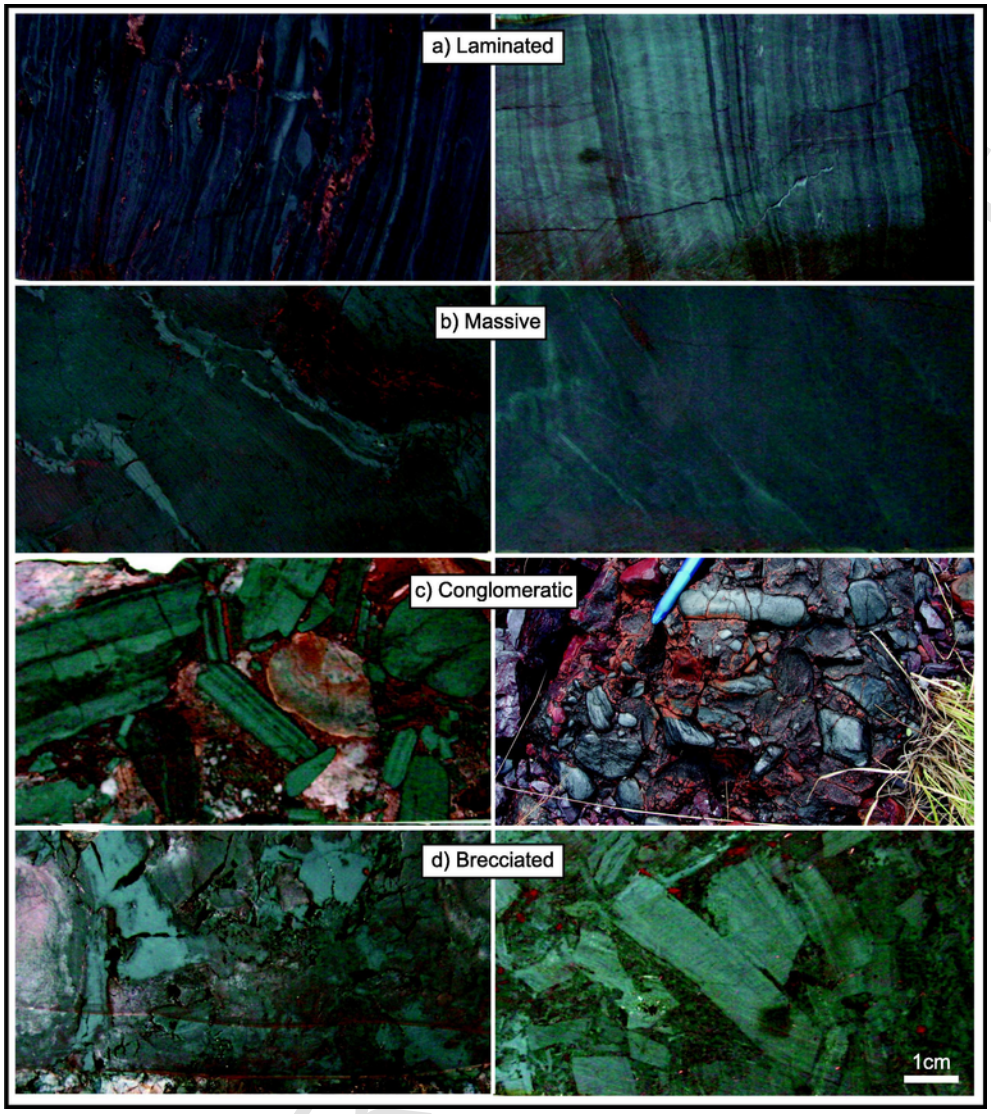

Fig. 3. Examples of ore types: (a) laminated ore comprising alternating microbands of higher- and lower-luster hematite, interspersed with hematite and specularite bands; (b) massive or clastic-textured ores are thickly bedded and contorted and are typically formed from the enrichment of muddy BIF; (c) conglomeratic ore, consisting of sub-rounded to angular hematite pebbles in a fine-grained hematite/specularite-rich matrix, typically formed by erosion of ore from higher-lying areas, followed by accumulation in depressions in the Gamagara Formation; (d) brecciated ore comprising very angular, poorly-sorted clasts of other ore types in a fine-grained matrix of hematite and quartz. Specularite is very common within the porous breccia matrix. Brecciated ore is thought to have resulted from the collapse of overlying supergene-enriched ore into karstic features that were formed by the dissolution of dolomite. Each core sample is ~5 cm in diameter.

(Fig. 3a). Within the upper portion of the Asbestos Hills Subgroup, finely-laminated hematite ore grades upwards into thickly-bedded or massive ore (Fig. 3b). According to Smith and Beukes (2016), the difference between laminated and massive ores is mainly due to the texture of their respective proto-ores: laminated ore is essentially enriched microbanded BIF (termed ferhythmite), whereas massive/clastic ore represents enriched clastic-textured muddy BIF (termed lutite) (see Beukes and Gutzmer, 2008 for BIF classification). Together, laminated and massive ore form the most important sources of high-grade, lump ore at Kolomela and in the region (Machaka, 2014). Most researchers (e.g. Van Schalkwyk and Beukes, 1986; Moore et al., 2001; Beukes et al., 2002; Carney and Mienie, 2003; Smith and Beukes, 2016) suggest that these ore types are derived from leaching of chert from BIF during supergene alteration. As such, high-grade hematite iron ore is apparently limited to sites where the regional pre-Gamagara/Mapedi unconformity, which is consistently marked by the presence of a ferruginous lateritic weathering profile in the rocks immediately below it, is situated on BIF. Reworked and clastic ores are generally higher in SiO_2, Al_2O_3, K_2O and TiO_2, apparently reflecting the incorporation of shale and possibly superimposed alteration events. Massive ore, which is traditionally grouped with clastic ore, is generally lower in P, which is a deleterious impurity for iron and steel manufacturing, as it causes intergranular fracture at low temperatures, thereby resulting in brittle steel (Abiko et al., 1995).

Conglomeratic ore consists of subrounded to angular hematite pebbles in a fine-grained hematite/specularite-rich matrix (Carney and Mienie, 2003; Fig. 3c). According to Smith and Beukes (2016), this ore type forms through erosion of enriched, relatively higher-lying BIF, followed by deposition in low-lying areas. Conglomeratic ore often lies on, or is found in close proximity to, the Gamagara unconformity. Carney and Mienie (2003) observed that conglomeratic ore of the Gamagara Subgroup's Doornfontein Conglomerate Member occurs within basinal and synclinal structures and on the downthrown side of major fault planes.

Brecciated ore (Carney and Mienie, 2003; Friese and Alchin, 2007; Smith and Beukes, 2016) consists of very angular, poorly-sorted clasts

of laminated, massive and conglomeratic ore in a fine-grained matrix of hematite and quartz (Fig. 3d). Angular fragments of BIF and argillitic material also occur in collapse breccias, in which specularite is very common within the porous breccia matrix. Brecciated ore is thought to have resulted from collapse of overlying supergene enriched ore into karstic features that were formed by the dissolution of dolomite by acidic fluids (see Smith and Beukes, 2016 for a detailed explanation of this process). According to Carney and Mienie (2003), at both Sishen and Kolomela, ore-bearing palaeosinkholes only occur on prominent antiformal or domal structures such as the Maremane and Wolhaarkop Domes, a setting that essentially encapsulates or typifies Ploegfontein, although the reader is referred to Basson et al. (2017) for additional observations on the importance of paleosinkholes. Brecciated ore also occurs on the downthrown side of major normal faults and within palaeosinkholes in Campbell Rand Subgroup carbonates, typically accompanied by shale and chert breccia.

All of the abovementioned ore types have been distinguished from hydrothermally-enriched ores which formed at the bottom contact between the host iron formation and underlying carbonaceous shale. Examples of these include Thabazimbi, situated in the Penge Iron Formation of the Transvaal Supergroup, within the northern portions of the outcrop area of the Transvaal Supergroup, within the metamorphic aureole of the Bushveld Complex (Basson and Koegelenberg, 2016). Kolomela is also apparently distinct from the Bovenzeekoebaart deposit and the magmatic-hydrothermal Nauga East deposit, which are hosted by the Kuruman Iron Formation of the Asbesheuwels Subgroup (Harding, 2004).

In 2003, Kolomela deposits contained laminated (52.9% of total), clastic-textured (28.8%), brecciated (9.8%) and conglomeratic (8.6%) ore (Carney and Mienie, 2003). A further 12 years of development and additional data have not significantly altered these proportions. Based on the modelling performed for this study, Kolomela contains 53.1% laminated, 28.9% clastic, 6.5% brecciated and 11.4% conglomeritic ore.

3. Methodology

3.1. Data sources

Mapping was undertaken at Kolomela in 2009, 2012, 2014 and 2015, resulting in a total of 3,388 data points for structural analysis and map compilation. The Leeuwfontein and Kapstevel Pits were comprehensively mapped, although only limited mapping was undertaken at Klipbankfontein in 2015. The remaining three deposits have yet to undergo overburden stripping. Mapping points were collated, validated and imported into ArcGIS, Micromine and LeapfrogGeo™ with the necessary coordinate and datum adjustments and translations between mine grid and the 3D modelling space. Other data sources incorporated into structural interpretations and 3D models included >5000 drillholes, comprising over 297,000 m of diamond core and 92,000 m of reverse air-bore or percussion drilling (Fig. 4). Fig. 4 displays these drillhole collars in the context of the model boundaries. Because drillholes are the primary data source forinterpretation, volumes containing less drillhole data are inherently not as well-constrained as volumes with dense drillhole data. Regional data includes medium-resolution geophysical data from the South African Council for Geoscience, high-resolution aerial photographs from low-level drone surveys and a mine-wide gravity survey.

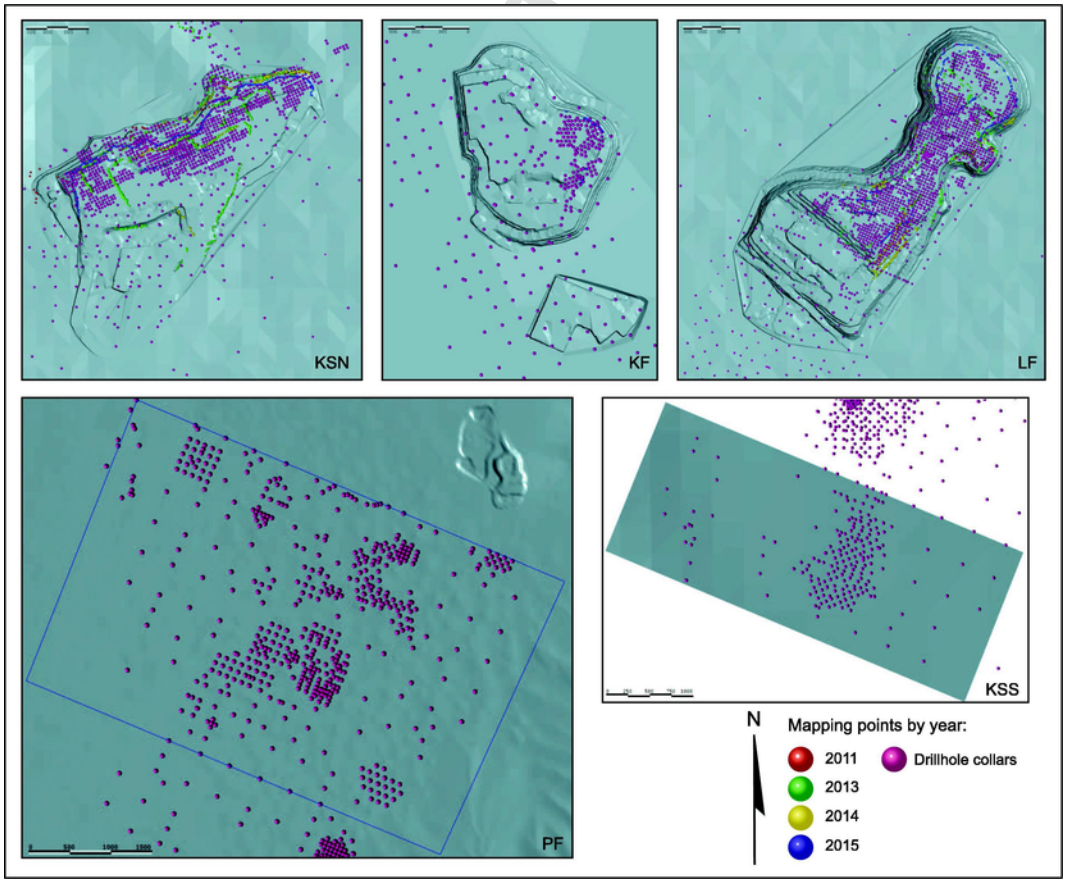

Fig. 4. Distribution of drillhole and mapping data within the five Kolomela deposits. Volumes encompassing less drilling and mapping are inherently of lower confidence than volumes encompassing dense drilling and mapping data.

3.2. Structural analysis

Based on this data and pit observations, three main types of faults occur at Kolomela:

3.2.1. NNE-SSW trending normal and inverted normal faults

Strike-extensive, NNE-SSW trending, steep, predominantly W-dipping normal and inverted normal faults are the dominant structural features at Kolomela Mine (Figs. 2, 5a, b, 7). These are identified primarily from notable offsets between adjacent, closely-spaced drillholes, mapping and distinct limonite staining. These faults are significantly more tightly spaced at the termination of the Maremane Dome and tend to be more concentrated within its western half, based on regional geophysical data and LandSat interpretations. At Leeuwfontein, NNE-trending normal faults, which show a dip direction and dip of 105°/83°, transect the length of the pit and accommodate the central trough or keel-like geometry of the deposit (Figs. 6b and 7c). Bedding orientations, for instance at Leeuwfontein, reflect rotation of blocks that are bounded by these faults, expressed by girdle segmentation (poles to bedding: Fig. 6a). Kapstevel North contains numerous, segmented, NNE-trending faults, with an orientation of approximately 136°/82° (Fig. 6d). Based on the average bedding orientation (Fig. 6c), there may be a set of earlier NW-dipping normal faults which were rotated, along with bedding, to more moderate dips. NNE-trending faults are defined in the pit by a networked zone of anastomosing fracture planes that show a great deal of internal variability in orientation. Individual faults contain calcite, sericite, fault gouge, clay, talc, epidote and fine-grained euhedral quartz, suggesting these were water-bearing, partially or completely open structures. Indeed, there appears to be a degree of hydraulic connectivity between Leeuwfontein and the adjacent Beeshoek Mine. Recent research indicates broadly N—S to NNW-SSE-trending ambient crustal shortening stresses (σ_1) and E-W extensional stresses (σ_3) (Bird et al., 2006; Delvaux and Barth, 2010). These stresses would dilate normal faults that are sub-parallel to the current σ_1, while structures at high angles to σ_1 would remain closed or would undergo transpression. Normal faults formed prior to the deposition of the Ghaap Group or deposition of Koegas Subgroup units at *c.* ~2.43–2.35 Ga, although the structural history, summarized in Table 1, suggests that they underwent numerous phases of reactivation, particularly during the Kalahari Orogeny and Kheis Orogeny.

3.2.2. NE/ENE- and NW/WNW-trending strike-slip faults and fractures

A series of NW-SE-trending, predominantly strike-slip faults, with a typical spacing of 600 m–1000 m, transect almost the entire mining area and offset normal faults, orebodies and segments of the Wolhaarkop Dome. These are particularly evident in Figs. 1 and 2. These faults were identified from ground gravity data acquired during the exploration stage, subsequently supported by detailed mapping. An interpretation of this data shows right-lateral offset of the gravity anomaly on which the Leeuwfontein Pit is established. Consequently, the straight southern edge of Leeuwfontein (Fig. 7c) is predicated on this NW-trending fault; their dominant orientation in the pit is 046°/80° (Fig. 6b; dip direction and dip), while at Kapstevel North this orientation is 053°/74° (Fig. 6d). Where discrete or well-defined, these faults show a small-scale to *meso*-scale anastomosing, brittle to brittle-ductile internal geometry with fault-fracture zones up to 8 m wide. Copious calcite, epidote and Fe-bearing minerals form on main fault surfaces and on more shallowly-dipping fault splays between these. These minerals are particularly prevalent where these faults cross-cut NNE-SSW trending normal and inverted normal faults, indicating a degree of hydraulic interconnectivity, which is supported by the delineation of fractured rock aquifers and compartments in hydrological modelling. ENE- and NE-trending faults originated with the development of the Ventersdorp Rift Basin at 2.6 Ga to 2.5 Ga and would have been reactivated between 1.73 Ga and 1.4 Ga, thereby undergoing transpression during the eastward-verging Kheis Orogeny, from 1.4 to 1.25 Ga. The ~1.35–1.0 Ga

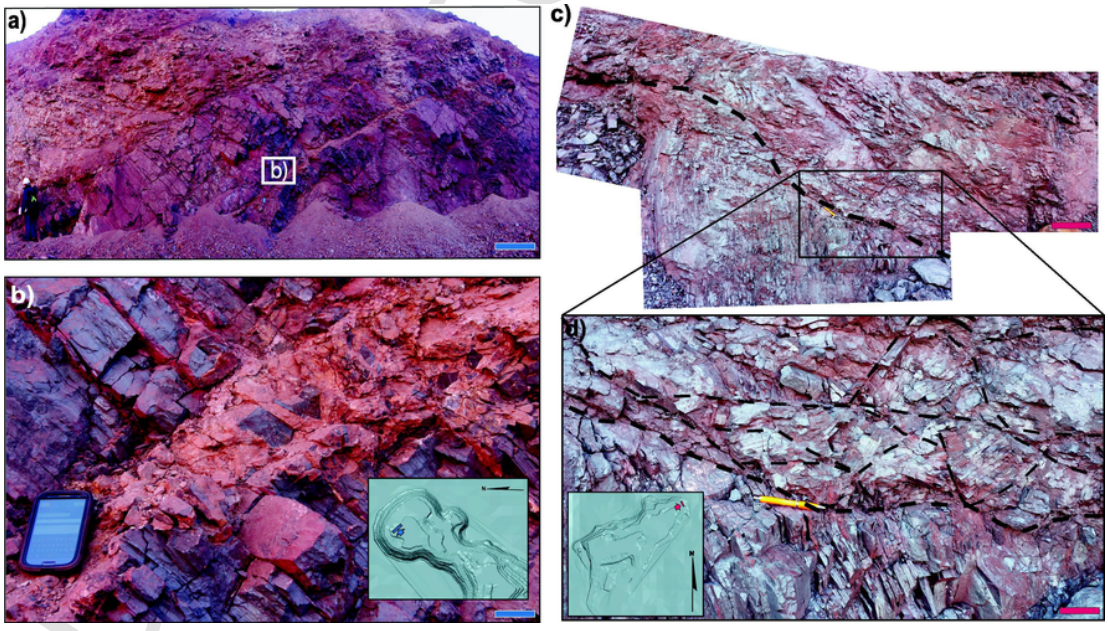

Fig. 5. (a) Large normal fault at LF which bounds the southern side of an ore block that tilts northwards, into the page and into a palaeosinkhole. The block contains distinct NE-SW trending major faults which, in this area, show the development of fault breccia and fault gouge (see b). (c) and (d) show a set of low-angle, anastomozing fault planes in laminated ore, at KSN. Due to the brittle nature of the rock, blocks have been fractured and rotated. (e) Cross-section from KSN, perpendicular to the primary axis of the Wolhaarkop Dome, showing predominantly SE-directed, low-angle or thin-skinned thrusting and fold vergence. Meso-scale structures include sympathetic cleavage, synthetic small-scale faults and closed to isoclinal folds (particularly in thick quartzite units). The overall SE-wards dip suggests refolding of the entire tectonostratigraphy and its contained thrusts. (f) Drag folds at the top of a bench at KSN, related to low-angle, SE-verging thrusting, which has affected shale and quartzite above ore. Low-angle thrusting has caused thickening and duplication of units, in this example, shale. (g) Thrust plane with entrained graphitic shale, enclosed within BIF of the Asbestos Hills Subgroup, in the northern end of LF pit. (h) SE-verging, recumbent, isoclinal fold defined by quartzite.

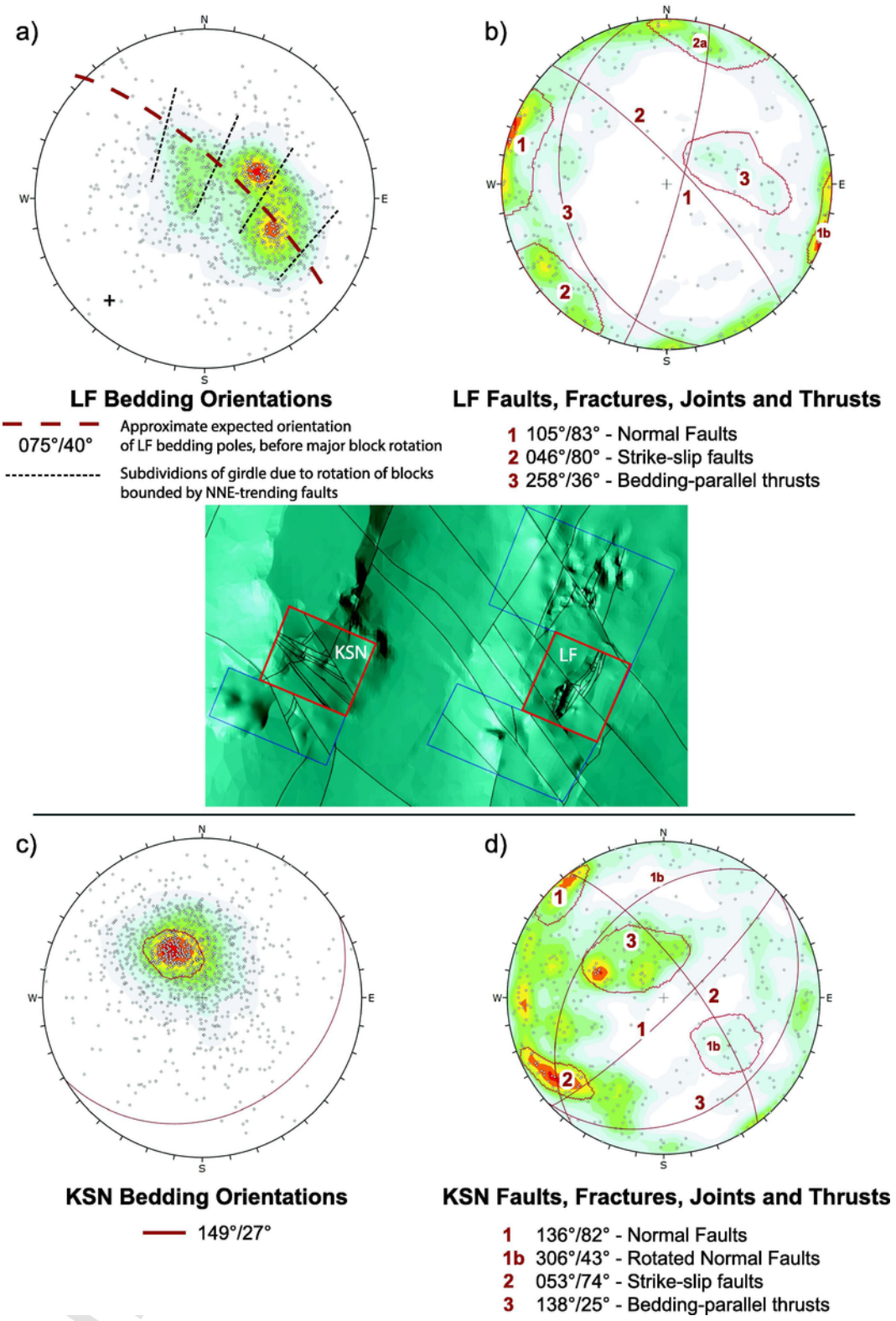

Fig. 6. Equal area, lower-hemisphere stereonets of mapping data recorded in the Leeuwfontein (a and b) and Kapstevel North (c and d) pits. Average orientations of each set are in dip direction/dip convention. See text for details.

NNW-directed Lomanian or Namaqua-Natal Orogeny would also have had an effect on this portion of the Maremane Dome (Altermann and Hälbich, 1990, 1991).

3.2.3. East-verging thrusting and associated features

The effects of thrusting are predominant in the Gamagara Formation and downwards through the stratigraphy (Fig. 5c–h). This is noted by Basson et al. (2017) in their study of Sishen Mine and Hilliard

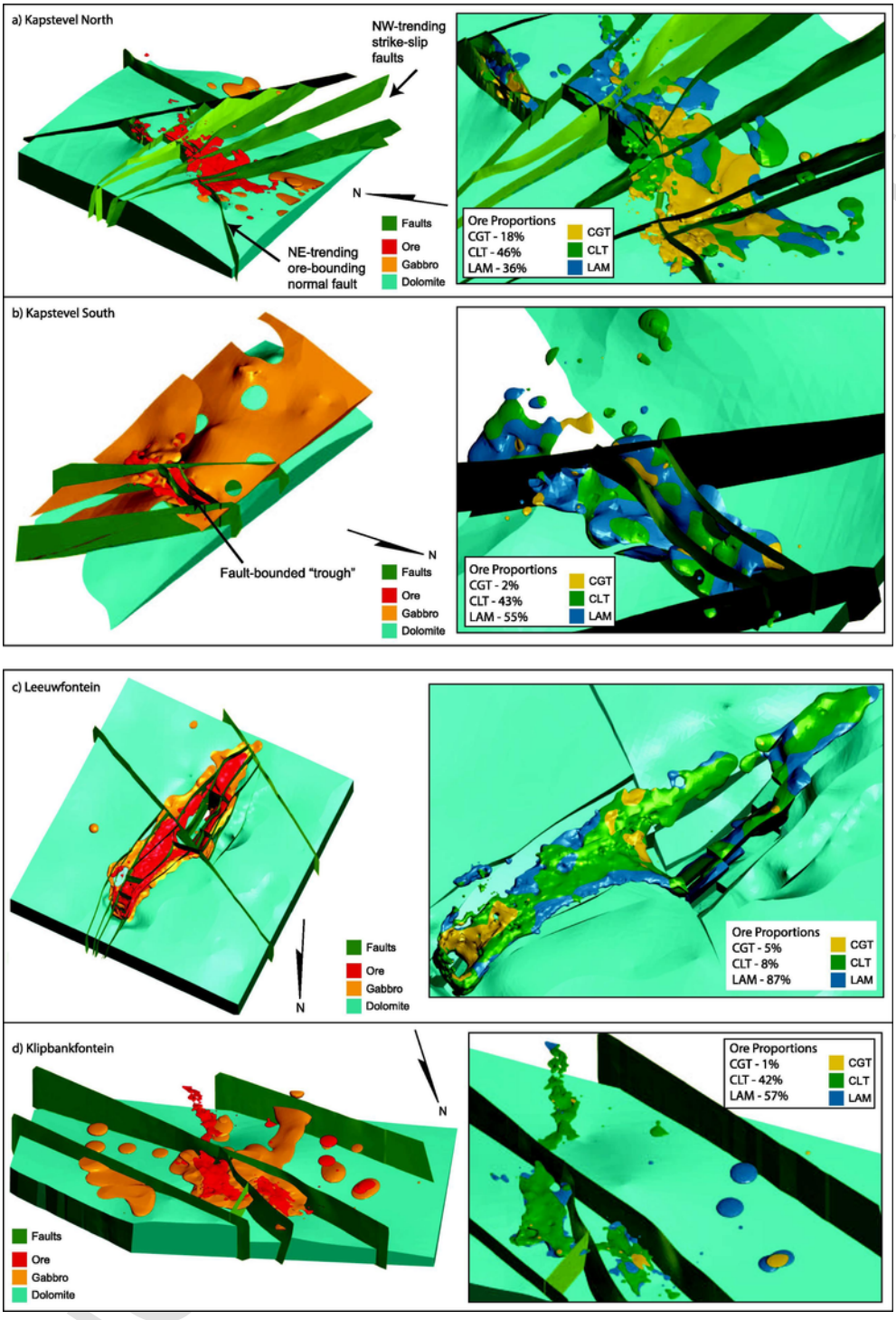

Fig. 7. Views of 3D models of each deposit within the Kolomela area. Left-hand images show dolomite, gabbro and ore solids as well as faults. Right-hand images display modelled laminated, clastic, conglomeritic and brecciated ore types, in the context of faults and the top contact of dolomite. Relative proportions of each ore type are given as a percentage of the total ore volume within each deposit (refer to Table 3).

(1999) in his study of the Griqualand West Supergroup wherein shearing along contacts, rotation of bedding in the vicinity of major thrusts and bedding sub-parallel simple shear in the Asbestos Hills and Koegas Subgroups were cited as common features. The effects of low-angle, E- to SE-verging, bedding-parallel thrusting (e.g. Fig. 5e) are more evident at the Kapstevel North and Leeuwfontein pits, due to their proximity to the Kheis orogenic front. Most shale-rich units, contacts between shale and more competent units such as internal quartzite lenses, and the shale-BIF-contact, exhibit low-angle, bedding-parallel or bedding-(sub)parallel movement, typically accompanied by the formation of proto-mylonite or mylonite and S—C cleavages within units. These collectively indicate eastward thrusting and tectonic vergence at a series of contacts or major, tectonized erosional unconformities. Duplication or stacking of BIF and underlying units is common in the NW face of Kapstevel North. Broad refolding of the entire sequence and its incorporated thrusts has resulted in shallowly SE-wards dipping thrusts

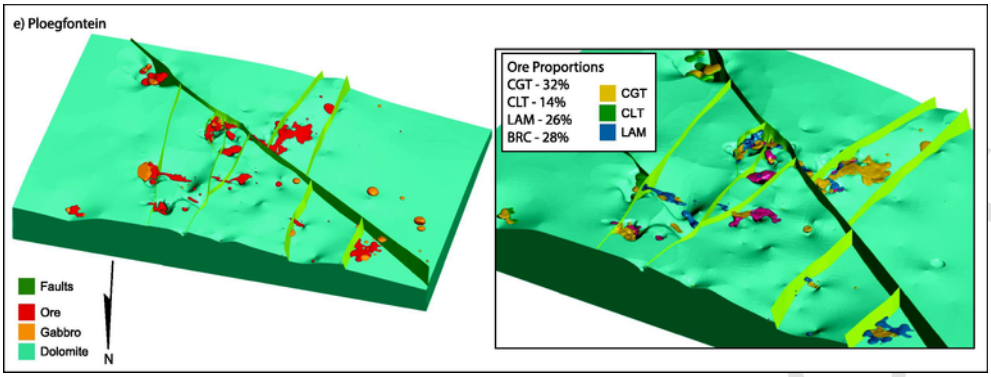

Fig. 7. (*Continued*)

in the Kapstevel North Pit (orientation of 138°/25°: Fig. 6d). The Kapstevel North Pit shows small-scale, NW-verging back-thrusts and accommodation faulting around fold hinge zones. Thrusting has caused the entrainment of carbonaceous or graphitic shale - similar to the Penge unit at Thabazimbi – from the top of the dolomite unit into BIF at Leeuwfontein (Fig. 5g).

3.3. Implicit model construction

Each mine-scale 3D model was constructed separately, with the regional structural network and the geometry of the top-dolomite surface as contextual backdrops. For each pit, faults were built as meshes in LeapfrogGeo™ using the regional geophysical data interpretation, pit mapping data and offsets between adjacent drillholes. Faults were locally adjusted by using guiding structural disks, polylines and surface meshes of previously-modelled faults. These faults were then combined into a structural network, through the application of crosscutting or terminating relationships, based on the orientation and timing of regional structural events. The fault network was used to divide each model into a series of individual, fault-bounded blocks, with an internal series of logical and validated lithological volumes.

Lithological modelling in LeapfrogGeo™ requires the creation of contact surfaces, which are then assigned age relationships and intersecting rules or conditions, to further subdivide the model volume or each fault-bounded block, into its constituent lithologies. Contact surfaces require unique contact points from drillhole logging or mapping data but, due to the geology at Kolomela as well as the variability in logging over an approximately 20-year period, unambiguous contacts are not always evident. Furthermore, the resultant model cannot represent the complexity of very detailed logging. Compounding issues include facies changes, combined with shearing along shale horizons and entrainment of carbonaceous and graphitic material along thrusts within BIF. Consequently, drillholes show "barcoding" (or repeated, alternating layers of different lithological units). In order to simplify these intervals, lithological logging codes were grouped into 11 primary lithological groups, representing broad stratigraphic units (see Table 2). Shorter intervals were removed through compositing, to resolve unique contact points. For ore, this interval thickness limit is generally 1.5 m, such that any isolated interval less than 1.5 m is not considered by the software for the generation of contact points. Intervals that could not be removed through compositing, or which are due to logging errors, were manually recoded and grouped with their appropriate enclosing unit.

Dolomite underlies the Kolomela area, but very few drillholes intersect it. Consequently, many fault blocks do not contain sufficient dolomite intersections for modelling a top-of-dolomite surface with the same resolution as stratigraphically-higher surfaces. In these cases, the regional top-dolomite surface, which was generated from geophysical data (Wooldridge and Hobson, 2015), was used for interpolation purposes. Where necessary, explicit guidance was introduced through the placement of *structural discs* between very deep drillhole intersections. Fig. 2 displays the outline of the 2015 model limits in the context of this regional dolomite surface.

Table 2
Lithological grouping of logging codes and the stratigraphic units they represent.

Model Lithology	Stratigraphic Unit
KALAHARI	Kalahari Group
TILLITE	Dwyka Formation
HEM	Asbestos Hills Subgroup, with Fe > 60%
GABBRO	Gabbro
LAVA	Ongeluk Formation
QTZ_CH	Gamagara Formation
QUARTZITE	Gamagara Formation
CONGLOMERATE	Gamagara Formation
GAMAGARA	Gamagara Formation
BIF	Asbestos Hills Subgroup
CHERT	Wolhaarkop Formation
DOL	Campbellrand Subgroup

Although most lithologies in the Kolomela area are sedimentary in origin, LeapfrogGeo™ models according to geometry, rather than origin or genesis. In order to obtain realistic shapes, more extensive lithologies are modelled as deposits, or erosional surfaces if their lower contacts are unconformable, while less-extensive or more discontinuous bodies such as conglomerate, quartzite and ore are modelled as "intrusions". Because these units form isolated or stacked lenses rather than extensive layers, an "intrusion" contact surface better accounts for their irregularity and discontinuity. The overall geometry of intrusion surfaces is controlled through the use of ellipsoid ratios, with a ratio such as 16:16:1 producing a much flatter and more extensive shape than a ratio of, for instance, 5:5:1. Ellipsoid ratios were determined for each surface by an iterative "best-fit" process. Very flat ellipsoid ratios were employed to connect the great majority of ore intersections and produce realistic, lens-shaped geometries. A primary modelled HEM volume was refined, in each model, into the three main ore types: viz. clastic (including massive), laminated and conglomeritic, based on an additional column that records secondary lithological and textural information.

4. 3D deposit descriptions

4.1. Setting and geometry

4.1.1. Kapstevel North

The Kapstevel North deposit (KSN) lies along the southwestern side of the NE-trending Wolhaarkop Dome, which parallels the southern termination of the nearby Maremane Dome (Figs. 1 and 2). A major, NE-

trending normal fault, running closely parallel to the northern edge of the pit, shows downthrow on its southern side (Fig. 7a). The majority of ore occurs predominantly on this downthrown side, in a partially-inverted graben or half-graben, accompanied by the formation of considerable conglomeritic material and conglomeratic ore. North of this fault, much of the stratigraphy has been eroded away, including most of the ore, due to relative uplift.

Regional geophysical data over the KSN area defines at least eight NW-SE-trending, strike-slip faults, which comprise one component of a regional conjugate joint/fault set (i.e. NW-SE and NE-SW). Due to refolding of the Maremane Dome (F_2?) and the influence of the *ca.* 1 Ga Namaqua-Natal event, these structures were reactivated, thereby offsetting N—S trending structures, grabens, half-grabens and their related lithological units. Not only do aeromagnetic images show extreme Fe enrichment along these faults near or at the Namaqua Belt, particularly along the Griquatown Fault Zone (see Altermann, 1997), but vertical movement along these faults has created a series of local, fault-bounded blocks, wherein ore is preserved. Consequently, a total of 18 activated faults sub-divide the volume into 22 fault-bounded blocks. Based on the available drillhole information and in contrast to the other deposits, KSN does not have gabbro underlying the ore.

4.1.2. Kapstevel South

Due to the limited number of drillholes and the absence of mapping data, only four faults are delineated. Two NE-trending normal faults bound a down-faulted block. These structures are truncated by two extensive, sub-vertical, NW-trending strike-slip faults (Fig. 7b). Thin intervals of conglomeratic material occur in the proximity of this trough, although a minority of this comprises conglomeratic ore. A NW-trending strike-slip structure is probably responsible for the left-lateral offset of KSN from KSS. Two well-defined, laterally-extensive gabbro sills, separated by a particularly thick BIF unit, are evident in cross-section (Fig. 8). Ore is predominantly preserved above both gabbro sills, while only minor ore volumes are preserved below the lower gabbro sill (Fig. 8). Ore also straddles the BIF-Gamagara contact, but is not limited to it, as drilling clearly shows thin intersections of BIF above ore, possibly suggesting that ore formation is not exclusively a supergene process at the upper BIF contact. Gabbro sills show dips and geometries that suggest their emplacement along low-angle thrusts, similar to that shown in Fig. 5g.

4.1.3. Leeuwfontein

Leeuwfontein (LF) is situated on the southern termination of the surface outcrop of the NE-trending Maremane Dome (Figs. 1 and 2). The dolomite contact is high in the area surrounding LF, while the palaeosinkhole-dominated Ploegfontein (PF) area occurs ~500 m to the north of LF. Several prominent NE-SW-trending structures run along the length of the LF Pit. These are essentially rift-, graben- or half-graben-related normal faults, which were inverted during subsequent or successive orogenies and effectively contributed to the formation of a doubly-plunging syncline within the crest of a broader anticlinal or domal structure. These normal faults show a cumulative downthrow (of ~450 m) towards the center of the deposit, thereby creating a "keel-like" geometry (Fig. 7c). Two major NW-SE-trending strike-slip faults offset these pre-existing normal or "longitudinal" faults. One of these strike-slip faults transects, and offsets, the orebody in a dextral sense at its approximate center. A substantial volume of conglomeratic ore is preserved in the northernmost end of the pit, due to the presence of a major palaeosinkhole that is superimposed on this "keel-like" geometry, wherein thick intervals of Gamagara Group shale, conglomerate and quartzite are preserved. Furthermore, a significant thickness of conglomeratic ore occurs to the north of the NW-SE trending normal fault through the center of the deposit (Fig. 7c).

A noticeable feature at LF is a thick gabbro sill that consistently underlies the ore volume (Figs. 7c, 8c and 10), occasionally separated by thin intersections of BIF. Where drillhole density is low, especially towards the edges of the model, gabbro intersections are present but could not reasonably be extrapolated between or beyond drillholes further than 200 m apart. It is nonetheless likely that additional gabbro is developed in the SE part of the model.

4.1.4. Klipbankfontein

The Klipbankfontein (KF) deposit lies to the south of the LF deposit. Lithologies are flat-lying and unaffected by superimposed karstification or paleosinkholes, although they generally thicken downdip toward the southeast, accompanied by an increase in the thickness of Ongeluk Lava and Gamagara shale (Fig. 8). Due to the limited exposure in the pit, the majority of modelled faults have been interpreted from regional geophysical data and downhole offsets between adjacent drillholes: four NW-SE trending structures, one of which also transects the LF model and a single, less extensive N—S trending structure which bounds the major ore volume on the west side (Fig. 7d). The relationship between ore and gabbro at LF is also present at KF, as the majority of ore is underlain by gabbro, although not all modelled gabbro volumes are overlain by ore.

4.1.5. Ploegfontein

Ploegfontein (PF) is situated further north than LF and KF, effectively on top of the southern arm of the exposed Maremane Dome. Consequently, dolomite is relatively close to the surface and the area displays numerous instances of karstification. BIF has almost completely been removed by erosion and is only preserved in palaeosinkholes and dolines (Fig. 8). A total of eight NE-SW trending faults transect the PF volume; these are either normal, reverse or inverted normal faults and are invariably steeply-dipping and tangential to the Maremane Dome's western margin (Figs. 1 and 2). These faults are offset by a major NW-trending strike-slip fault. The majority of ore is found in palaeosinkholes, adjacent to faults or in dolines along these. Palaeosinkholes in PF's central portion host significant volumes of downthrown HEM blocks (Fig. 7e), accompanied by brecciated chert, BIF, Gamagara Group sediments and gabbro. This may suggest that the relationship between gabbro and ore, prior to the formation of karstic features, was also important at PF.

5. Discussion

5.1. Ore type and gabbro distribution

Examining the 3D models of the five main Kolomela deposits, it is clear that although they all contain the same ore types, generally in the same vertical sequence (laminated ore grading upwards into clastic ore, with conglomeritic ore above this) the distribution and relative proportions of these ore types vary greatly from one deposit to another, as does the amount of brecciated ore (Fig. 7).

A large percentage (18%) of ore at KSN is conglomeratic, while LF and KF contain only 5% and 1% of conglomeritic ore, respectively. KSS and PF both contain relatively low volumes of conglomeritic ore. In keeping with the ore type sequence, conglomeritic ore at KSN lies on top of the other two ore types, typically where the total ore thickness is high, along the southwestern, downthrown side of the NE-trending normal fault that delimits the pit's northern extent (Fig. 5a). KSS contains predominantly laminated and clastic ore but, according to available drilling, these ore types (in contrast to LF) are intermingled (Fig. 7b). At LF, clastic-textured ore is "enclosed" in the underlying laminated ore, due to the synclinal shape of the deposit, while conglomeratic ore lies predominantly in and around the major palaeosinkhole at the pit's northern extremity and along the major dextral strike-slip fault that

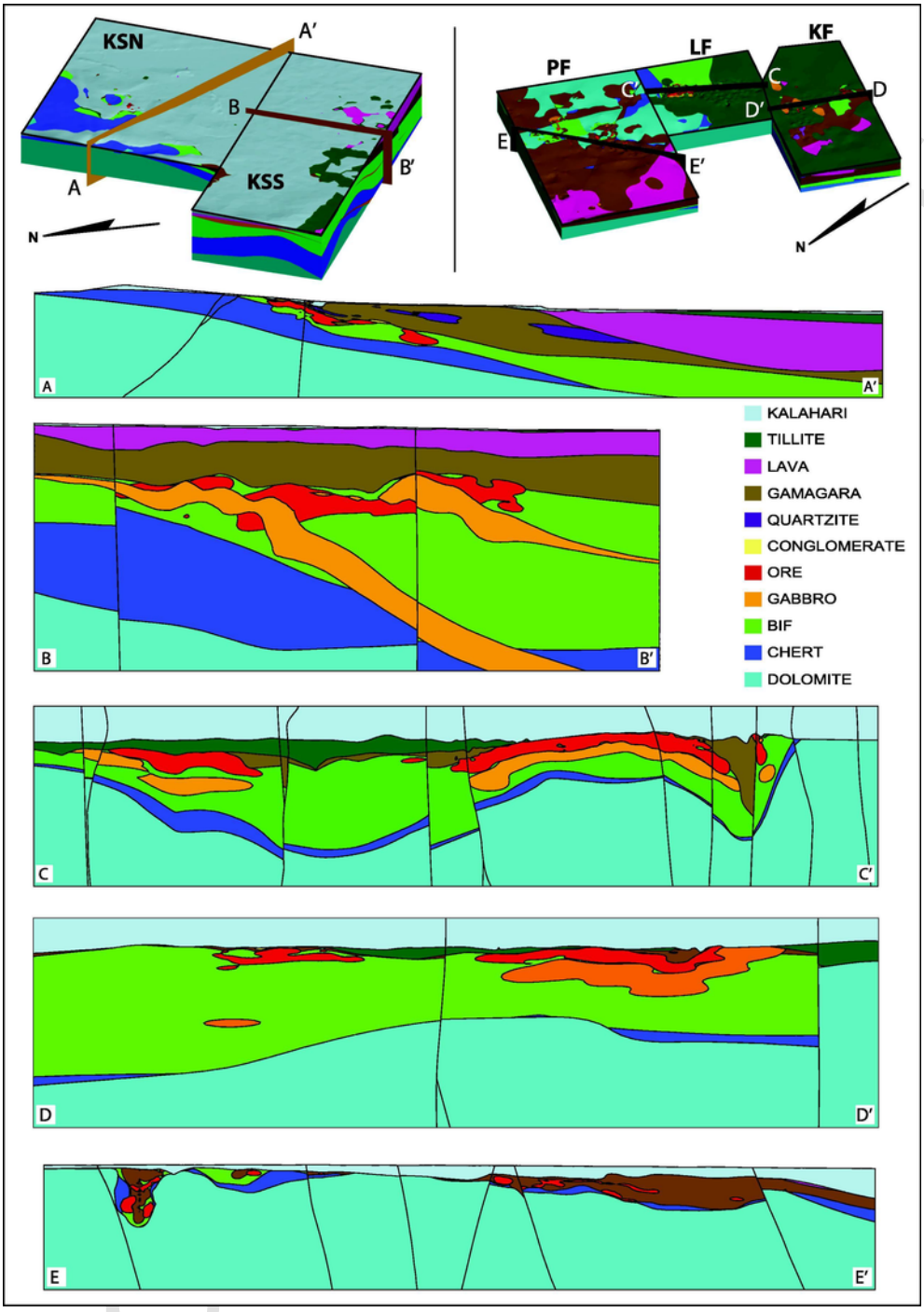

Fig. 8. Across-strike cross-sections through 3D models of KSN, KSS, PF and KF. The LF section is parallel to the main axis of the synclinal structure that hosts the deposit.

transects the orebody (Fig. 7c). KF is perhaps the least "disturbed" deposit, as ore types are highly stratified, laminated ore dominates and there is very little conglomeratic ore, although there is a comparatively high proportion of clastic-textured ore (Fig. 7d). At PF, ore is predominantly preserved in deeply-karstified, shallow dolomite and, in accordance with this, constitutes a far greater proportion of conglomeritic (32%) and brecciated (28%) ore, compared to laminated (26%) or clastic ore (14%; Fig. 7e).

3D models of the Kolomela deposits have also revealed the geometry, extent and position of thick gabbro bodies and their relation to ore bodies. Thick gabbro sills occur to the south of KSN and underlie the majority of ore at KSS, LF and KF. Large blocks of gabbro are preserved alongside large blocks of ore in PF paleosinkholes. In terms of timing, Gous (2012) found that due to the presence of ore xenoliths as well as enrichment of gabbro in Fe, gabbro is interpreted to have intruded during, or after, the latter stages of mineralisation (at *c.* 2430 Ma; Gous, 2012), although this assumes only one stage of predominantly supergene Fe enrichment and this relationship remains to be confirmed by formal age dating. At KSS and LF, thick, laterally extensive gabbro sills follow the shape of the synclinal/graben geometry, and were therefore subject to the same faulting and folding as ore. At KSS, its two gabbro sills dip to the south, in an orientation similar to that of the low-angle thrust in BIF at LF (see Fig. 5g). As the upper and/or lower contacts of gabbro exhibit extreme alteration and the formation of local skarns, it

seems likely that gabbro intruded along low-angle thrusts that contained entrained carbonaceous/graphitic shale and dolomite.

To better define the relationship between gabbro sills and high-grade iron ore, thickness plots were created from gabbro and ore wireframes, on a 10 m × 10 m grid, used to generate contact points. The vertical distance between these contact points is effectively an apparent thickness. The results are displayed in Fig. 9, with cooler colours representing thinner areas and hotter colours representing thicker areas, for each wireframe. A histogram was also generated for thickness data in each deposit, to indicate the range and distribution of ore and gabbro apparent thicknesses, which are close to their true values. These statistics are also summarized for each deposit and ore type in Table 3. Fig. 9 shows that there is a strong spatial correlation between, firstly, the location of ore and an underlying, proximal gabbro sill: in LF, KSS and KF ore is almost always underlain by gabbro (Fig. 10). Secondly, ore appears to be extremely thick above intervals of very thick gabbro (Fig. 9). However, there are numerous instances of gabbro that are not overlain by ore; KSS, for example, contains extensive gabbro sills which cover most of the model area, and yet ore is only found in and around the nearby graben structure. KSN is the exception, as it contains very little gabbro and almost none of it is below ore. However, while ore in

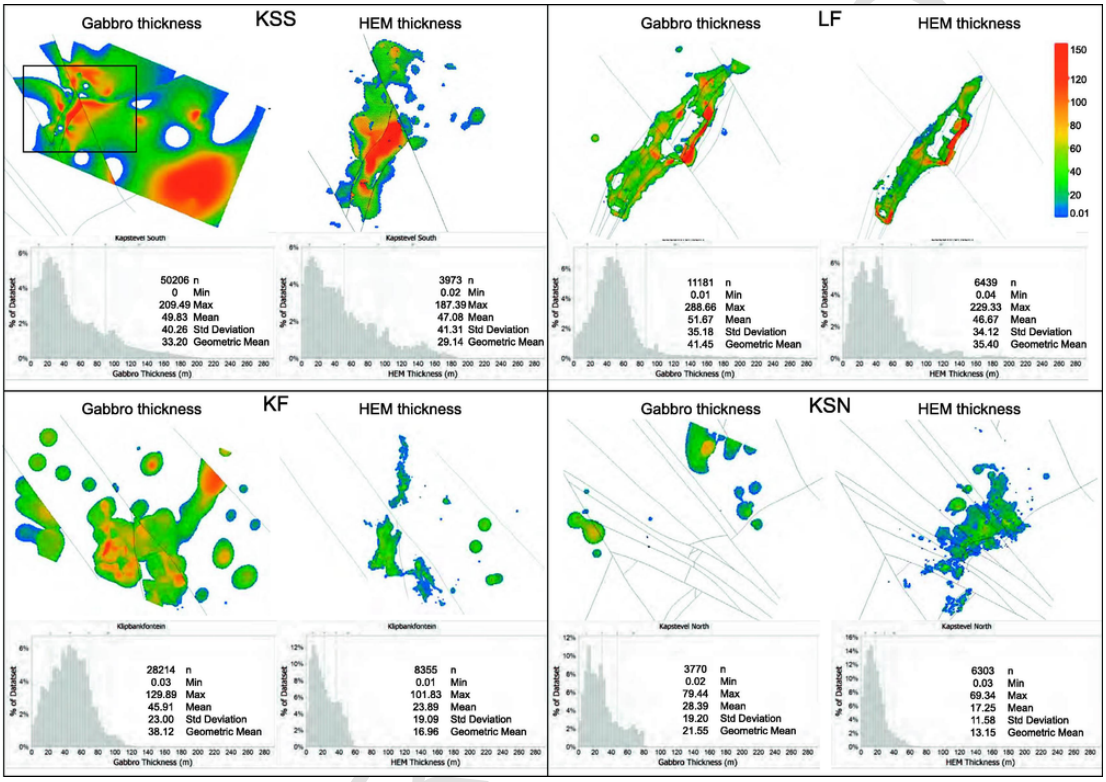

Fig. 9. Contoured data on a point grid (10 m x 10 m spacing), showing the apparent, vertical thickness of modelled ore and gabbro wireframes. Cooler colours represent thinner intersections and hotter colours represent thicker intersections. Histograms for each deposit indicate range and distribution of apparent thickness of gabbro and ore. In most deposits, with the exception of KSN, there is a strong spatial correlation between thicker ore and thicker, typically underlying, proximal gabbro in the form of sills.

Table 3
Summary of ore and gabbro thickness data.

Deposit Name	Type	N	Min Thickness (m)	Max Thickness (m)	Mean	Standard Deviation	Geometric Mean
KSS	LAM	2896	0	152.93	38.67	31.58	24.59
	CLT	2159	0	165.39	40.4	37.55	24.38
	CGT	347	0.05	39.33	10.51	7.85	7.21
	HEM	3973	0.02	187.39	47.08	41.31	29.14
	GAB	50,206	0	209.49	49.83	40.26	33.20
KF	LAM	5723	0.02	101.83	20.82	20.02	13.91
	CLT	5448	0	58.26	16.04	10.59	12.13
	CGT	394	0.05	17.95	5.64	4.18	3.79
	HEM	8355	0.01	101.83	19.09	19.09	16.96
	GAB	28,214	0.03	129.89	45.91	23.00	38.12
LF	LAM	4968	0.05	181	33.79	26.7	26.62
	CLT	4640	0.02	180.38	29.51	23.39	20.78
	CGT	725	0.01	105.09	14.28	12.89	9.52
	HEM	6439	0.04	229.33	46.67	34.12	35.4
	GAB	10,962	0.01	288.66	51.67	35.18	41.45
KSN	LAM	3561	0	53.33	11.01	8.28	7.81
	CLT	3821	0	62.46	13.11	12.3	7.51
	CGT	2474	0.01	38.31	7.84	6.49	5.1
	HEM	6303	0.03	69.34	17.25	11.58	13.15
	GAB	3770	0.02	79.44	28.39	19.20	21.55

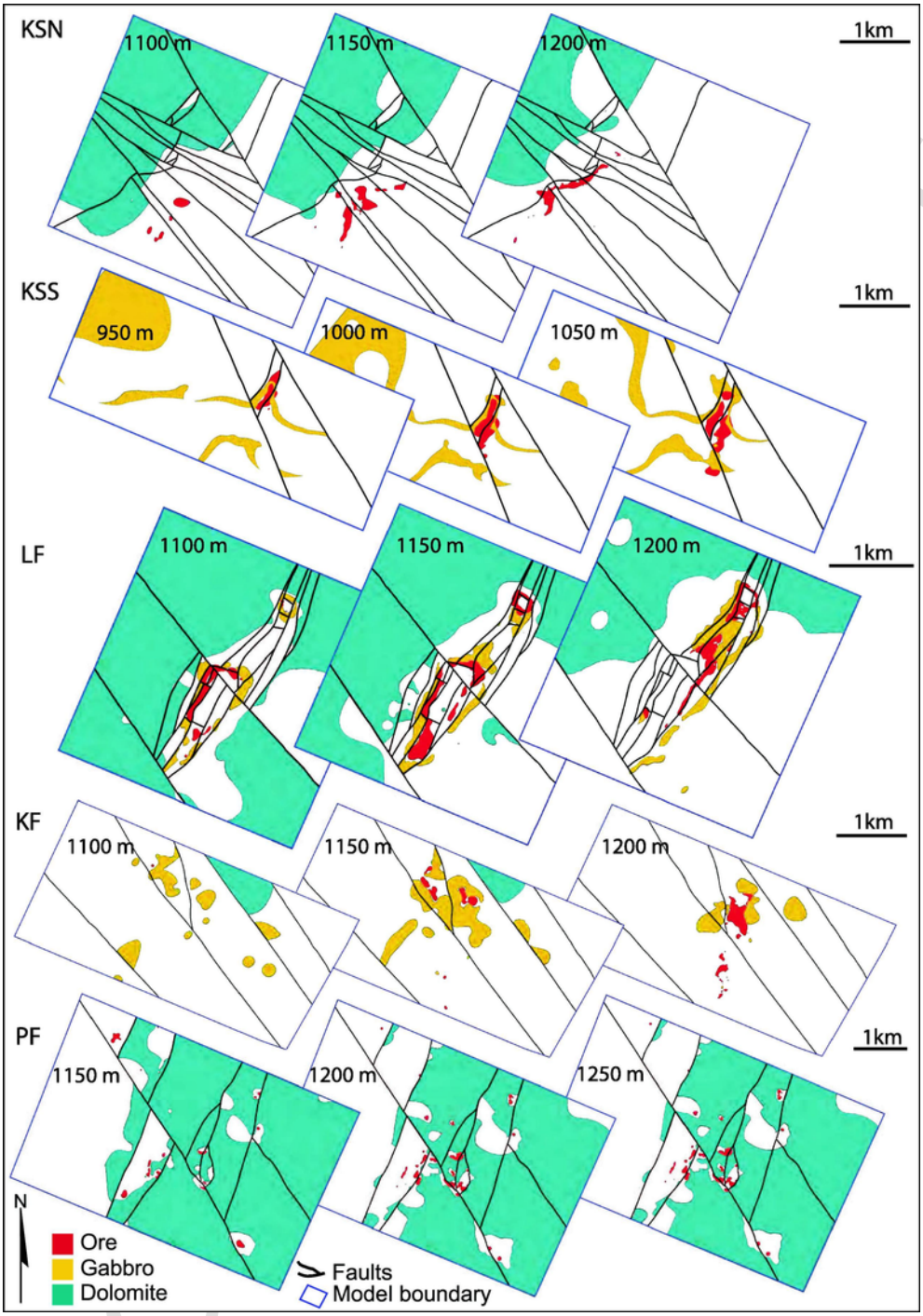

Fig. 10. Successive depth slices through the various 3D models, displaying ore, gabbro, dolomite and their bounding and cross-cutting faults. Most depth slices are horizontal, with the exception of those at Kapstevel South, which have an orientation of 135°/06°, approximately parallel to the top-dolomite and base-lava surfaces.

the other deposits may locally exceed thicknesses of 200 m, KSN ore has a maximum thickness of ~70 m.

Mapping, closely-spaced drilling and fully-constrained 3D modelling undertaken for this study demonstrate that ore types at Kolomela are variable over short distances. Ore types also reflect the interaction of faults with underlying dolomite and the level of the BIF-Gamagara contact, and the influence of proximal, thick gabbro sills that intruded along contacts and low-angle thrusts.

5.2. Genetic models

Hagemann et al. (2016) propose a multi-faceted approach to considering the genesis of a BIF-hosted iron ore system. A number of controls need to be considered: tectonic controls, pathways for hydrothermal fluids from source to deposition, the structural framework and architecture of these depositional sites, introduction of alteration minerals, sources and characteristics of hydrothermal fluids (hypogene and supergene) and subsequent ore preservation, uplift and either final or

intermittent supergene modification. The tectonic setting of Kolomela Mine, to the east of the leading thrust of the Kheis Orogenic Front that has affected a thick sedimentary package, allows for the possibility that factors other than supergene enrichment have contributed to mineralisation. Land et al. (2017), in their study of the basal Mapedi Formation of the Olifantshoek Supergroup and the unconformity with the Ongeluk Formation, describe pronounced enrichment in HFSE (Ti, Nb, Y, Zr, REE, etc.), compared to average shale, accompanied by K-metasomatism and transgressive Fe-oxidation, which they ascribe to post-depositional fluid-rock interaction involving Fe-bearing diagenetic brines. They propose that such fluids may be responsible for alteration, enhanced Fe mobility and development of epigenetic hematitic iron ores along the regional Transvaal-Olifantshoek unconformity (see also Beukes et al., 2002).

Tsikos et al. (2003), in their study of the Hotazel Formation of the Kalahari manganese fields in close proximity to Sishen Mine, documented the geochemical effects of an isotopically-light, meteoric or low-temperature hydrothermal fluid, in the oxidation, leaching and enrichment of iron. They proposed that extensive fluid flow in the Kalahari manganese field was related to the Hotazel/Olifantshoek unconformity, at the top of the Transvaal/Griqualand West Supergroup, which is above the stratigraphic location of Sishen Mine. Papadopoulos (2016)'s petrographical investigation into the Manganore Iron Formation demonstrated that high-grade iron ore is formed through multi-stage alteration events dominated by hydrothermal activity. Fe and Si mobility and metasomatic alteration were attributed to layer-controlled fronts, which were interconnected with the Kuruman and Griquatown iron formations. This study furthermore concludes that metals, S and C were sourced from the underlying dolomite and that the BIF-Gamagara Shale contact probably acted as a fluid conduit for the development of high-grade haematitic ore. Therefore, large-scale, possibly hydrothermal fluid metasomatism also needs to be considered as being instrumental in the mineralisation or upgrading process in the Maremane Dome Area.

Other models invoke hydrothermal fluids, related to basinal dewatering or the circulation of basinal brines during regional-scale thrusting, thereby leaching silica and precipitating secondary hematite. McLellan et al. (2003) and Dalstra and Rosière (2008) highlight the importance of normal faults and thrusts which, when accompanied by far-reaching, gravity-driven fluid flow, may generate large, crustal, hydrodynamic systems. Extensional inversion, also documented at this edge of the Kaapvaal Craton (Table 1), would have involved underpressure and dilation and would have enabled downward fluid migration. McLellan et al. (2003)'s models, based on their observations, are applicable not only to ore genesis in the Hamersley Province but to other extensional environments, in sedimentary basins with depths of 2–8 km, and the shallower portions of orogenic belts.

Angerer et al. (2014) state that high-grade, BIF-hosted Fe deposits, regardless of their size or scale, represent a combination of multiple, structurally-controlled diagenetic, metamorphic, hypogene hydrothermal and typically supergene modification/enrichment events. Several genetically-distinct episodes of iron ore formation, producing heterogeneous orebodies with highly variable proportions of goethite, hematite and magnetite-rich ore are apparent in large, high-grade (>55 wt% Fe), BIF-hosted deposits such as those in the Hamersley Province (e.g. Mt. Tom Price deposit; Taylor et al., 2001) and the Yilgarn Craton (e.g. Koolyanobbing deposits; Angerer and Hagemann, 2010). Alteration involves changes in the iron oxide mineralogy and textures, producing distinct alteration zones with quantifiable distal-intermediate-proximal iron oxide–silicate–carbonate, de-silicification and de-carbonatisation signatures which either "prepare" the volume for mineralisation or increase the porosity of high-grade iron ore. While predominantly structurally-controlled hydrothermal alteration of BIF and surrounding country rocks is described in nearly all major iron districts, the presence and the extent of these effects are becoming increasingly apparent in areas close to Kolomela (e.g. Papadopoulos, 2016). In the Thabazimbi area (Basson and Koegelenberg, 2016), enhanced hydrothermal fluid flow and significant iron mineralisation were attributed to thrusting and shearing, combined with fold amplification and flexural flow along the E-W trending detachment between the Malmani dolostone and banded iron formation. In particular, fold-accommodation structures such as conjugate shear joints, normal and reverse faults and thrusts, and Fe localization at intersections of major reverse faults, detachments and stratigraphically-higher low-angle thrusts all played a role in Fe enrichment.

Regarding the presence and role of mafic intrusions, hydrothermal alteration of these bodies at Mt. Tom Price and Paraburdoo are suitable analogues for gabbroic intrusions at Kolomela (Taylor et al., 2001; Thorne et al., 2004). In these Australian deposits, dykes cross-cut and entrain BIF and high grade ore, but also follow the contact between ore and BIF in a manner similar to that at Kolomela. Further similarities include a large degree of alteration, with dykes comprising chlorite (pseudomorph after pyroxene and amphiboles), talc (pseudomorph after feldspars) and accessory leucoxene and pyrite (Taylor et al., 2001; Thorne et al., 2004). Based on Fe enrichment and a comparison of the geochemical signatures of Fe mineralisation and mafic dykes, the latter were found to be emplaced prior to, or with, silica leaching, with the conclusion that mineralisation or further upgrading occurred late in the structural evolution.

6. Conclusions

Kolomela Mine cannot be considered to be a direct analogue of Sishen Mine. Rather, Kolomela hosts a series of deposits which display widely varying characteristics, as well as various structural geometries, degrees of preservation and reworking. This results in variable proportions of laminated, clastic and conglomeratic ore, with the latter typically occurring in close proximity to major definable structures, particularly normal faults that bound grabens or half-grabens. While ore generally straddles the Gamagara-BIF contact, it is not limited to it, with drillhole intersections of BIF occurring between ore and Gamagara (Fig. 8b).

The protracted, multi-phase tectonic evolution, complete with several compressional-extensional events, at this margin of the Kaapvaal Craton, would have provided an ideal setting for "preparation" of BIF by early low-grade metamorphism, deformation and porosity creation, followed by fluid movement along interconnected lithological contacts and unconformities, gabbro contacts and major structures. Researchers such as Hagemann et al. (2016), Angerer et al. (2014) and Lascelles (2002) have highlighted the important role of structures and their effect on multi-stage upgrading of Fe mineralisation over protracted periods. Detailed pit-mapping and the construction of fully-constrained 3D models has confirmed the presence of important structural features in all of the main mineralised volumes at Kolomela Mine, including 1) Pre-mineralisation structures that typically allow the movement of fluid during *syn*-mineralisation reactivation of faults, either during compression or extension (e.g. McLellan et al., 2003, 2004), including normal faults in the underlying basement and volcano-sedimentary units (Table 1); 2) Syn-ore structures, such as reactivated normal faults (i.e. KSN; see also Li et al., 2011) and constrictional or fold-accommodation structures within amplified folds previously recorded elsewhere in highly deformed portions of the same basin (Basson and Koegelenberg, 2016); 3) Syn-ore structures or movement along older structures that produce collapse breccia and thereby induce porosity (i.e. PF) and 4) Post-ore structures that modify, segment and locally preserve pre-existing ore bodies (Basson et al., 2017) and 5) Extensive permeable, horizontal or subhorizontal surfaces, which allowed for lat-

eral movement of fluids but prevented vertical fluid movement (i.e. the pre-Gamagara unconformity surface and the contacts of gabbro sills).

The 3D models of Kolomela deposits demonstrate a strong spatial correlation between thicker gabbro and thicker ore. While gabbro sills are clearly not a pre-requisite for ore formation or preservation, it is possible that they acted as relatively impermeable lithological surfaces or unconformities, in a manner similar to that described by Tsikos et al. (2003), Papadopoulos (2016) and Land et al. (2017), during fluid movement events, subsequently augmented by supergene enrichment. Further quantitative study into the timing of gabbro is needed to establish how large a role it may have played in ore creation, enrichment and preservation.

Uncited references

Bau (1993), Beukes and Gutzmer (1998), Krapež et al. (2003), Ohmoto et al. (2006), Van Schalkwyk (1984).

References

Abiko, K., Liu, C.-M., Ichikawa, M., Suenaga, H., Tanino, M., 1995. Effect of phosphorus on hot ductility of high purity iron. Journal de Physique IV France 5 (C7), 335–340.

Alchin, D.J., Botha, W.J., 2005. The structural/stratigraphic development of the Sishen South (Welgevonden) iron ore deposit, South Africa, as deduced from ground gravity data modelling. In: Proceedings Iron Ore 2005 Conference. The Australasian Institute of Mining and Metallurgy, Melbourne, pp. 29–41.

Alchin, D., Lickfold, V., Mienie, P.J., Nel, D., Strydom, M., 2008. An integrated exploration approach to the Sishen South iron ore deposit, Northern Cape Province, South Africa, and its implication for developing a structural and/or resource model for these deposits. In: In: Hagemann, S., Rosière, C., Gutzmer, J., Beukes, N.J. (Eds.), Reviews in Economic Geology Vol. 15, Society of Economic Geologists, Littleton, pp. 317–338.

Altermann, W., 1997. Sedimentological evaluation of Pb-Zn exploration potential of Precambrian Griquatown Fault Zone in the Northern Cape Province, South Africa. Mineralium Deposita 32, p362–p391.

Altermann, W., Hälbich, I.W., 1990. Thrusting, folding and stratigraphy of the Ghaap Group along the southwestern margin of the Kaapvaal Craton. S. Afr. J. Geol. 93, 553–556.

Altermann, W., Hälbich, I.W., 1991. Structural history of the southwestern corner of the Kaapvaal Craton and the adjacent Namaqua realm: new observations and a reappraisal. Precambr. Res. 52 (1), 133–166.

Angerer, T., Hagemann, S.G., 2010. The BIF-hosted high-grade iron ore deposits in the Archean Koolyanobbing Greenstone Belt, Western Australia: Structural control on synorogenic- and weathering-related magnetite-, hematite-, and goethite-rich iron ore. Econ. Geol. 105, 917–945.

Angerer, T., Duuring, P., Hagemann, S.G., Thorne, W., McCuaig, T.C., 2014. A mineral system approach to iron ore in Archaean and Palaeoproterozoic BIF of Western Australia. Geological Society of London Special, Publication, 393.

Armstrong, R.A., 1987. Geochronological studies on Archaean and Proterozoic formations of the foreland of the Namaqualand front and possible correlates on the Kaapvaal Craton: Unpublished Ph.D. dissertation, University of the Witwatersrand, Johannesburg, South Africa, p. 274.

Basson, I.J., Koegelenberg, C., 2016. Structural controls on Fe mineralisation at Thabazimbi Mine, South Africa. Ore Geol. Rev. 80, 1056–1071.

Basson, I.J., Anthonissen, C.J., McCall, M.J., Stoch, B., Britz, J., Deacon, J., Strydom, M., Cloete, E., Botha, J., Bester, M., Nel, D., 2017. Ore-structure relationships at Sishen Mine, Northern Cape, Republic of South Africa, based on fully-constrained implicit 3D modelling. Ore Geol. Rev. 86, 825–838.

Barley, M.E., Pickard, A.L., Hagemann, S.G., Folkert, S.L., 1999. Hydrothermal origin for the 2 billion year old Mount Tom Price giant iron ore deposit, Hamersley province, Western Australia. Miner. Deposita 34, 784–789.

Barton, E.S., Altermann, W., Williams, I.S., Smith, C.B., 1994. U-Pb zircon age for a tuff in the Campbell Group, Griqualand West Sequence, South Africa: Implications for Early Proterozoic rock accumulation rates. Geology 22, 343–346.

.

Bekker, A., Holland, H.D., Wang, P.-L., Rumble III, D., Stein, H.J., Hannah, J.L., Coetzee, L.L., Beukes, N.J., 2004. Dating the rise of atmospheric oxygen. Nature 427, 117–120.

Bekker, A., Slack, J.F., Planavsky, N., Krapez, B., Hofmann, A., Konhauser, K.O., Rouxel, O.J., 2010. Iron formation: the sedimentary product of a complex interplay among mantle, tectonic, oceanic, and biospheric processes. Econ. Geol. 105, 467–508.

Beukes, N.J., 1983. Paleoenvironmental setting of iron-formations in the depositional basin of the Transvaal Supergroup, South Africa. In: Trendall, A.C. and Morris, R.C., (eds.), Iron-Formation: facts and problems. Developments in Precambrian Geology, 6, Elsevier, Amsterdam, 131–209, 558 pp.

Beukes, N.J., Smit, C.A., 1987. New evidence for thrust faulting in Griqualand West, south Africa; implications for stratigraphy and the age of red beds. S. Afr. J. Geol. 90 (4), 378–394.

, .

Beukes, N.J., Gutzmer, J., Mukhopadhyay, J., 2002. The geology and genesis of high-grade hematite iron ore deposits. In: Proceedings Iron Ore 2002 Conference, pp 23–29 (The Australasian Institute of Mining and Metallurgy: Melbourne); Published in Applied Earth Science IMM Transactions section B.

Beukes, N.J., Gutzmer, J., 2008. Origin and paleoenvironmental significance of major iron formations at the Archaean-Paleoproterozoic boundary. In: In: Hagemann, S., Rosière, C., Gutzmer, J., Beukes, N.J. (Eds.), Reviews in Economic Geology Vol. 15, Society of Economic Geologists, Littleton, pp. 5–47.

Bird, P., Ben-Avraham, Z., Schubert, G., Andreoli, M., Viola, G., 2006. Patterns of stress and strain rate in southern Africa. J. Geophys. Res. 111, B08402.

Boardman, L.G., 1948. The geology of iron ore and other minerals of the Thabazimbi area. Unpublished Ph.D. Thesis, Pretoria University, p. 225.

Carney, M., Mienie, P., 2003. Comparison of the Sishen and Sishen South (Welgevonden) iron ore deposits, Northern Cape Province, South Africa. Appl. Earth Sci. (Trans. Inst. Min. Metall. B) 112(B5).

Cornell, D.H., Schütte, S.S., Eglington, B.L., 1996. The Ongeluk basaltic andesite formation in Griqualand West, South Africa: Submarine alteration in a 2222 Ma Proterozoic sea. Precambr. Res. 79, 101–123.

Cornell, D.H., Zack, T., Andersen, T., Corfu, F., Frei, D., van Schindel, V., 2016. The U-Pb zircon geochronology of the Palaeoproperozoic Hartley formation porphyry by six methods with age uncertainty approaching 1 Ma. S. Afr. J. Geol. 119 (3), 473–494.

Du Preez, J.W., 1944. The structural geology of the area east of Thabazimbi and the genesis of the associated ore. Ann. Univ. Stellenbosch 22A, 264–360.

Dalstra, H.J., Rosière, C.A., 2008. Structural controls on high-grade iron ores hosted by banded iron formation: a global perspective. Rev. Econ. Geol. 15, 73–106.

Delvaux, D., Barth, A., 2010. African stress pattern from formal inversion and focal mechanism data. Tectonophysics 482, 105–128.

De Villiers, J.E., 1944. The origin of the iron and manganese deposits in the Postmasburg and Thabazimbi area. Trans. Geol. Soc. South Afr. 47, 123–135.

de Villiers, P.R., Visser, J.N.J., 1977. The glacial beds of the Griqualand West Supergroup as revealed by four deep boreholes between Postmasburg and Sishen. Trans. Geol. Soc. South Afr. 80, 1–8.

Eriksson, P.G., Schweitzer, K., Bosch, P.J.A., Schereiber, U.M., Van Deventer, J.L., Hatton, C.J., 1993. The Transvaal sequence: an overview. J. Afr. Earth Sc. 16 (1–2), 25–51.

Erikson, P.G., Altermann, W., Hartzer, F.J., 2006. The Transvaal Supergroup and its precursors. In: Johnson, M.R., Anhaeusser, C.R., Thomas, R.J. (Eds.), The Geology of South Africa. Geological Society of South Africa. Johannesburg/Council for Geoscience, Pretoria, p. 238.

Fairey, B., Tsikos, H., Corfu, F., Polteau, S., 2012. U-Pb systematics in carbonates of the Postmasburg Group, Transvaal Supergroup, South Africa: primary versus metasomatic controls. Precambr. Res. 231, 194–205.

Findlay, D., 1994. Diagenetic boudinage, an analogue model for the control of hematite enrichment of iron ores of the Hamersley iron province of Western Australia and a comparison with Krivoi Rog of Ukraine and the Nimba Range, Liberia. Ore Geol. Rev. 9, 311–324.

Friese, A.E.W., Alchin, D.J., 2007. New insights into the formation, structural development, and preservation of iron ore deposits in the Northern Cape Province, South Africa. In: Proceedings Iron Ore 2005 Conference, The Australasian Institute of Mining and Metallurgy.

Gous, C.C., 2012. Igneous Intrusion within the Stratigraphy of Kolomela mine. Unpublished Honours Thesis, University of the Free State, Bloemfontein, p. 62.

Gross, G.A., 1993. Industrial and genetic models for iron ore in iron-formations. In: Kirkham, R.V., Sinclair, W.D., Thorpe, R.I., Duke, J.M. (Eds.), Mineral Deposit Modelling, Special Paper 40, Geological Association of Canada, pp. 151–170.

Gutzmer, J., Beukes, N.J., 1998. The manganese formation of the Neoproterozoic Penganga Group, India - Revision of an enigma. Econ. Geol. Bull. Soc. Econ. Geol. 93 (7), 1091–1102.

Gutzmer, J., Mukhopadhyay, J., Beukes, N.J., Pack, A., Hayashi, K., Sharp, Z.D., 2006. Oxygen isotope composition of hematite and genesis of high-grade BIF-hosted iron ores. Geol. Soc. Am. Mem. 198, 257–268.

Gutzmer, J., Chisonga, B.C., Beukes, N.J., Mukhopadhyay, J., 2008. The geochemistry of banded iron formation-hosted high-grade hematite-martite iron ores. Rev. Econ. Geol. 15, 157–183.

Hagemann, S.G., Angerer, T., Duuringa, P., Rosière, Figueiredo e Silva, R.C., Lobato, L., Hensler, A.S., Walde, D.H.G., 2016. BIF-hosted iron mineral system: a review. Ore Geol. Rev. 76, 317–359.

Hälbich, I.W., Scheepers, R., Lamprecht, D.F., van Deventer, J.L., De Kock, N.J., 1993. The Transvaal-Griqualand West banded iron formation: geology, genesis, iron exploitation. J. Afr. Earth Sc. 16, 63–120.

Harding, C.J., 2004. Origin of the Zeekoebaart and Nauga East high grade iron ore deposits, northern Cape Province, South Africa. Unpublished M.Sc. thesis, Rand Afrikaans University, p. 123.

Hartnady, C.J.H., Joubert, P., Stowe, C.W., 1985. Proterozoic crustal evolution in southwestern Africa. Episodes 8, 236–245.

Hilliard, P., 1999. Structural evolution and tectonostratigraphy of the Kheis Orogen and its relationship to the south western margin of the Kaapvaal Craton. Unpublished Ph.D. Thesis, University of Durban-Westville, p. 235.

Kampmann, T.C., 2012. U-Pb geochronology and paleo-magnetism of the Westerberg sill, Kaapvaal Craton – support for a coherent Kaapvaal-Pilbara block (Vaalbara), M.Sc. Thesis, Lund University, Sweden, p. 36.

, .

Land, J.S., Tsikos, H., Cousins, D., Luvizotto, G., Zack, T., 2017. Origin of red beds and paleosols in the Palaeoproterozoic Transvaal and Olifansthoek Supergroups of South Africa: provenance versus metasomatic controls. Geol. J., (In Press). doi:10.1002/gj.2885.

Lascelles, D.F., 2002. A new look at old rocks: a non-supergene origin for BIF-derived in situ high-grade iron ore deposits, Proceedings Iron Ore 2002. Australasian Institute for Mining and Metallurgy, Perth, 107–126.

Lascelles, D.F., 2007. Genesis of the Koolyanobbing iron ore deposits, Yilgarn Province, WA, Australia. Appl. Earth Sci. (Trans. Inst. Min. Metall. B) 116(2), 86–93.

Lascelles, D.F., 2012. Banded iron formation to high-grade iron ore: a critical review of supergene enrichment models. Aust. J. Earth Sci. Int. Geosci. J. Geol. Soc. Aust. 59 (8), 1105–1125.
Li, N., Frei, M., Altermann, W., 2011. Textural and knowledge-based lithological classification of remote sensing data in Southwestern Prieska sub-basin, Transvaal Supergroup, South Africa. J. Afr. Earth Sc. 60, 237–246.
Machaka, E., 2014. A Comparison of Estimation Methods for Evaluating Iron Ore Bodies. Unpub. M.Sc. Thesis, University of the Witwatersrand, p. 150.
McLellan, J.G., Oliver, N.H.S., Ord, A., Zhang, Y., Schaubs, P.M., 2003. A numerical modelling approach to fluid flow in extensional environments: implications for genesis of large microplaty hematite ores. J. Geochem. Explor. 78–79, 675–679.
McLellan, J.G., Oliver, N.H.S., Schaubs, P.M., 2004. Fluid flow in extensional environments; numerical modelling with an application to Hamersley iron ores. J. Struct. Geol. 26, 1157–1171.
Moore, M., Tsikos, H., Polteau, S., 2000. Deconstructing the Transvaal Supergroup. J. Afr. Earth Sc. 31 (Suppl. 1A), 52–53.
Moore, J.M., Tsikos, H.A.N.D., Polteau, S., 2001. Deconstructing the Transvaal Supergroup, South Africa: implications for Palaeoproterozoic palaeoclimate models. J. Afr. Earth Sc. 33, 437–444.
Moore, J.M., Kuhn, B.K., Mark, D.F., Tsikos, H., 2011. A sugilite-bearing assemblage from the Wolhaarkop Breccia, Bruce Fe-ore mine, South Africa: evidence for alkali metasomatism and Ar40-Ar39 dating. Eur. J. Mineral. 23, 661–673.
Mortimer, B., 1995. Report on Structural Geological Analysis: Sishen. Internal Company Report, p. 71.
Papadopoulos, V., 2016. Mineralogical and geochemical constraints on the origin, alteration history and metallogenic significance of the Manganore iron-formation, Northern Cape Province, South Africa. Unpublished M.Sc Thesis, Rhodes University, p. 217.
Ramanaidou, E.R., Morris, R.C., 2010. Comparison of supergene mimetic and supergene lateritic iron ore deposits. Appl. Earth Sci. 119, 35–39.
Rasmussen, B., Zi, J-W., Sheppard, S., Muhling, J.R., 2016. Multiple episodes of hematite mineralisation indicated by U-Pb dating of iron-ore deposits, Marquette Range, Michigan, USA. Geol. Soc. Am. 44 (7), 543–546.
Rosière, C.A., Spier, C.A., Rios, F.J., Suckau, V., 2008. The itabirites of the Quadrilátero Ferrífero and related high-grade iron ore deposits: An overview. Rev. Econ. Geol. 15, 223–254.
Schlegel, G.C., 1988. Contribution to the metamorphic and structural evolution of the Kheis Tectonic Province, Northern Cape, South Africa. S. Afr. J. Geol. 91 (1), 27–37.
Schütte, S.S., 1992. Ongeluk volcanism in relation to the Kalahari manganese deposits: Unpublished Ph.D. dissertation, Durban, University of Natal, South Africa, p. 255.
Semami, F.B., De Kock, M., Soderlund, U., Gumsley, A., Da Silva, R., Beukes, N., Armstrong, R., 2016. New U-Pb geochronologic and palaeomagnetic constraints on the late Palaeoproterozoic Hartley magmatic event: evidence for a potential large igneous province in the Kaapvaal Craton during Kalahari assembly, South Africa. GFF (J. Geol. Soc. Sweden) 138 (1), 164–182.
Smith, A.J.B., Beukes, N.J., 2016. Palaeoproterozoic banded iron formation-hosted high-grade hematite iron ore deposits of the Transvaal Supergroup, South Africa. Episodes 39, 269–284.
Steynfaard, D.J., Louw, W.C., Kotze, J., Smith, J. Havenga, B.H.J., 2003. New developments on mine planning and grade control at Sishen Iron Ore Mine. J. S. Afr. Inst. Mining Metallurgy, Jan/Feb, 53–62.
Stowe, C.W., 1986. Synthesis and interpretation of structures along the north-eastern boundary of the Namaqua tectonic province, South Africa. S. Afr. J. Geol. 89 (2), 185–198.
Strauss, C.A., 1964. The iron ore deposits at Thabazimbi, Transvaal. In: Haughton, S.H. (Ed.), Geology of Some Ore Deposits of Southern Africa: Johannesburg. Geological Society of South Africa, South Africa, pp. 383–392.
Sumner, D.Y., Bowring, S.A., 1996. U-Pb geochronologic constraints on deposition of the Campbellrand Subgroup, Transvaal Supergroup, South Africa. Precambr. Res. 79, 25–35.
Taylor, D., Dalstra, H.J., Harding, A.E., Broadbent, G.C., Barley, M.E., 2001. Genesis of high-grade hematite orebodies of the Hamersley Province, Western Australia. Econ. Geol. 96, 837–873.
Thomas, R.J., Cornell, D.H., Moore, J.M., Jacobs, J., 1994. Crustal evolution of the Namaqua-Natal Metamorphic Province, southern Africa. S. Afr. J. Geol. 97, 8–14.
Thorne, W.S., Hagemann, S.G., Barley, M., 2004. Petrographic and geochemical evidence for hydrothermal evolution of the North deposit, Mt.Tom Price, Western Australia. Mineralium Deposita 39, 766–783.
Tinker, J., de Wit, M., Grotzinger, J., 2002. Seismic Stratigraphic Constraints on Neoarchean – Paleoproterozoic Evolution of the Western Margin of the Kaapvaal Craton, South Africa. S. Afr. J. Geol. 105 (2), 107–134.
Trendall, AF., Compston, W., Williams, I.S., Armstrong, R.A, Arndt, N.T., McNaughton, N.J., Nelson, D.R., Barley, M.E., Beukes, N.J., De Laeter, J.R., Retief, E.A., Tome, A.M., 1990. Precise zircon U-Pb chronological comparison of the volcano-sedimentary sequences of the Kaapvaal and Pilbara Cratons between about 3.1 and 2.4 Ga. Abstracts 3rd Int. Archaean symposium, Perth, pp. 81–83.
Tsikos, H., Beukes, N.J., Harris, C., Moore, J.M., 2003. Deposition, diagenesis and secondary enrichment of metals in the Palaeoproterozoic Hotazel iron-formation, Kalahari Manganese Field, South Africa. Econ. Geol. 98, 1449–1462.
Van Deventer, W.F., 2009. Textural and geochemical evidence for a supergene origin of the Paleoproterozoic high-grade BIF-hosted iron ores of the Maremane Dome, Northern Cape Province, South Africa. MSc dissertation (unpubl.), University of Johannesburg, Johannesburg, p. 107.
Van Deventer, J.L., Eriksson, P.G., Snyman, C.P., 1986. The Thabazimbi iron ore deposits, north-western Transvaal. In: Anhaeusser, C.R., Maske, S. (Eds.), Mineral Deposits of Southern Africa, I. Geological Society of South Africa, pp. 923–929.
Van Schalkwyk, J.F., Beukes, N.J., 1986. The Sishen iron ore deposit, Griqualand West. In: Anhaeusser, C.R., Maske, S. (Eds.), Mineral Deposits of Southern Africa. Geol. Soc. S. Afr, Johannesburg, pp. 931–956.
Van Wyk, J.P., 1980. Die geologie van die Rooinekke-Matsap-Wolhaarkop in Noord-Kaapland met spesiale verwysing na die Koegas Subgroup en die Transvaal Supergroep. M.Sc. Dissertation (unpubl.), Randse Afrikaans University, Johannesburg, South Africa, p. 159.
Visser, J.N.J., 1971. The deposition of the Griquatown Glacial Member in the Transvaal Supergroup. Trans. Geol. Soc. S. Afr. 74, 187–199.
Walraven, F., Burger, A.J., Allsopp, H.L., 1982. Summary of age determinations carried out during the period April 1980 to March 1981. Ann. Geol. Surv. S. Afr. 16, 107–114.
Wooldridge, A.M., Hobson, V., 2015. Kolomela Area Itasca Model. Internal Company Report for Kumba Iron Ore. p. 12.